1

Introduction

In this opening chapter, we give an informal and qualitative overview – a pep talk – to help you appreciate why sustained nonequilibrium systems are so interesting and worthy of study.

We begin in Section 1.1 by discussing the big picture of how the Universe is filled with nonequilibrium systems of many different kinds, a consequence of the fact that the Universe had a beginning and has not yet stopped evolving. A profound and important question is then to understand how the observed richness of structure in the Universe arises from the property of not being in thermodynamic equilibrium. In Section 1.2, a particularly well studied nonequilibrium system, Rayleigh–Bénard convection, is introduced to establish some vocabulary and insight regarding what is a nonequilibrium system. Next, in Section 1.3, we extend our discussion to representative examples of nonequilibrium patterns in nature and in the laboratory, to illustrate the great diversity of such patterns and to provide some concrete examples to think about. These examples serve to motivate some of the central questions that are discussed throughout the book, e.g. spatially dependent instabilities, wave number selection, pattern formation, and spatiotemporal chaos. The humble desktop-sized experiments discussed in this section, together with theory and simulations relating to them, can also be regarded as the real current battleground for understanding nonequilibrium systems since there is a chance to compare theory with experiment quantitatively.

Next, Section 1.4 discusses some of the ways that pattern-forming nonequilibrium systems differ from the low-dimensional dynamical systems that you may have seen in an introductory nonlinear dynamics course. Some guidelines are also given to determine qualitatively when low-dimensional nonlinear dynamics may not suffice to analyze a particular nonequilibrium system. In Section 1.5, a strategy is given and explained for exploring nonequilibrium systems. We explain why fluid dynamics experiments have some advantages over other possible experimental systems and why certain fluid experiments such as Rayleigh–Bénard convection are

especially attractive. Finally, Section 1.6 mentions some of the topics that we will *not* address in this book for lack of time or expertise.

1.1 The big picture: why is the Universe not boring?

When people look at the world around them or peer through telescopes at outer space, a question that sometime arises is: why is there something rather than nothing? Why does our Universe consist of matter and light rather than being an empty void? While this question remains unanswered scientifically and is intensely pursued by researchers in particle physics and cosmology, in this book we discuss a second related question that is also interesting and fundamental: why does the existing matter and light have an interesting structure? Or more bluntly: why is the Universe not boring?

For it turns out that it is not clear how the existence of matter and light, together with the equations that determine their behavior, produce the extraordinary complexity of the observed Universe. Instead of all matter in the Universe being clumped together in a single black hole, or spread out in a featureless cloud, we see with our telescopes a stunning variety of galaxies of different shapes and sizes. The galaxies are not randomly distributed throughout space like molecules in a gas but are organized in clusters, the clusters are organized in super-clusters, and these super-clusters themselves are organized in voids and walls. Our Sun, a fairly typical star in a fairly typical galaxy, is not a boring spherical static ball of gas but a complex evolving tangled medium of plasma and magnetic fields that produces structure in the form of convection cells, sunspots, and solar flares. Our Earth is not a boring homogeneous static ball of matter but consists of an atmosphere, ocean, and rocky mantle that each evolve in time in an endless never-repeating dynamics of weather, water currents, and tectonic motion. Further, some of the atoms on the surface of our Earth have organized themselves into a biosphere of life forms, which we as humans particularly appreciate as a source of rich and interesting structure that evolves dynamically. Even at the level of a biological organism such as a mammal, there is further complex structure and dynamics, e.g. in the electrical patterns of the brain and in the beating of the heart.

So again we can ask: why does the matter and light that exist have such interesting structure? As scientists, we can ask further: is it possible to explain the origin of this rich structure and how it evolves in time? In fact, how should we define or quantify such informal and qualitative concepts such as "structure" or "patterns" or "complexity" or "interesting?" On what details does this complexity depend and how does this complexity change as various parameters that characterize a system are varied?

While this book will explain some of what is known about these questions, especially at the laboratory level which allows controlled reproducible experiments, we can say at a hand-waving level why the Universe is interesting rather than boring: the Universe was born in a cosmological Big Bang and is still young when measured in units of the lifetime of a star. Thus the Universe has not yet lasted long enough to come to thermodynamic equilibrium: *the Universe as a whole is a nonequilibrium system*. Because stars are young and have not yet reached thermodynamic equilibrium, the nuclear fuel in their core has not yet been consumed. The flux of energy from this core through the surface of the star and out into space drives the complex dynamics of the star's plasma and magnetic field. Similarly, because the Earth is still geologically young, its interior has not yet cooled down and the flux of heat from its hot core out through its surface, together with heat received from the Sun, drives the dynamics of the atmosphere, ocean, and mantle. And it is this same flux of energy from the Earth and Sun that sustains Earth's intricate biosphere.

This hand-waving explanation of the origin of nonequilibrium structure is unsatisfactory since it does not lead to the quantitative testing of predictions by experiment. To make progress, scientists have found it useful to turn to desktop experimental systems that can be readily manipulated and studied, and that are also easier to analyze mathematically and to simulate with a computer. The experiments and theory described in this book summarize some of the systematic experimental and theoretical efforts of the last thirty years to understand how to predict and to analyze such desktop nonequilibrium phenomena. However, you should appreciate that much interesting research remains to be carried out if our desktop insights are to be related to the more complex systems found in the world around us. We hope that this book will encourage you to become an active participant in this challenging endeavor.

1.2 Convection: a first example of a nonequilibrium system

Before surveying some examples that illustrate the diversity of patterns and dynamics in natural and controlled nonequilibrium systems, we first discuss a particular yet representative nonequilibrium system, a fluid dynamics experiment known as Rayleigh–Bénard convection. Our discussion here is qualitative since we wish to impart quickly some basic vocabulary and a sense of the interesting issues before turning to the examples discussed in Section 1.3 below. We will return to convection many times throughout the book, since it is one of the most thoroughly studied of all sustained nonequilibrium systems, and has repeatedly yielded valuable experimental and theoretical insights.

A Rayleigh–Bénard convection experiment consists of a layer of fluid, e.g. air or water, between two horizontal plates such that the bottom plate is warm and

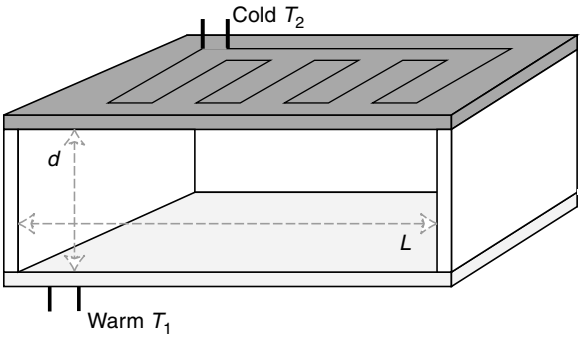

Fig. 1.1 Rayleigh–Bénard convection of a fluid layer between two horizontal plates is one of the simplest sustained nonequilibrium systems. The drawing shows a featureless square room of lateral width L and height d with copper-covered floor and ceiling, and supporting walls made of wood. By appropriate plumbing and control circuits, the floor and ceiling are maintained at constant temperatures of T_1 and T_2 respectively. When the temperature difference $\Delta T = T_1 - T_2$ is sufficiently large, the warm less-dense air near the floor and the cold more-dense air near the ceiling spontaneously start to move, i.e. convection sets in. The rising and falling regions of air eventually forms cellular structures known as convection rolls. The characteristic roll size is about the depth d of the air.

the upper plate is cool. As an example to visualize (but a bit impractical for actual experimentation as you will discover in Exercise 1.5), consider a square room whose lateral width L is larger than its height d, and in which all furniture, doors, windows, and fixtures have been removed so that there is only a smooth flat horizontal floor, a smooth flat horizontal ceiling, and smooth flat vertical walls (see Fig. 1.1). The floor and ceiling are then coated with a layer of copper, and just beneath the floor and just above the ceiling some water-carrying pipes and electronic circuits connected to water heaters are arranged so that the floor is maintained at a constant temperature T_1 and the ceiling is maintained at a constant temperature T_2.[1] Because copper conducts heat so well, any temperature variations within the floor or within the ceiling quickly become negligible so that the floor and ceiling can be considered as time-independent constant-temperature surfaces. The supporting sidewalls are made of some material that conducts heat poorly such as wood or Plexiglas.

A typical nonequilibrium experiment for the room in Fig. 1.1 would then be simply to fix the temperature difference $\Delta T = T_1 - T_2$ at some value and then to observe what happens to the air. "Observe what happens" can mean several

[1] Uniformly warming the floor and cooling the ceiling is not the usual way that a room is heated. Instead, a convector – a localized heat source with a large surface area – is placed somewhere in the room, and heat is lost through the windows instead of through the ceiling. (What we call a convector everyone else calls a radiator but this is poorly named since the air is heated mainly by convection, not by radiation.) But this nonuniform geometry is more complicated, and so less well suited, than our idealized room for experiment and analysis.

things depending on the questions of interest. By introducing some smoke into the room, the pattern of air currents could be visualized. A more quantitative observation might involve recording as a function of time t some local quantity such as the temperature $T(\mathbf{x}_0, t)$ or the x-component of the air's velocity $v_x(\mathbf{x}_0, t)$ at a particular fixed position $\mathbf{x}_0 = (x_0, y_0, z_0)$ inside the room. Alternatively, an experimentalist might choose to record some global quantity such as the total heat $H(t)$ transported from the floor to the ceiling, a quantity of possible interest to mechanical engineers and architects. These measurements of some quantity at successive moments of time constitute a time series that can be stored, plotted, and analyzed. A more ambitious and difficult observation might consist of measuring multivariate time series, e.g. measuring the temperature field $T(\mathbf{x}, t)$ and the components of the velocity field $\mathbf{v}(\mathbf{x}, t)$ simultaneously at many different spatial points, at successive instants of time. These data could then be made into movies or analyzed statistically. All of these observations are carried out for a particular fixed choice of the temperature difference ΔT and over some long time interval (long enough that any transient behavior will decay sufficiently). Other experiments might involve repeating the same measurements but for several successive values of ΔT, with each value again held constant during a given experiment. In this way, the spatiotemporal dynamical properties of the air in the room can be mapped out as a function of the parameter ΔT, and various dynamical states and transitions between them can be identified.

The temperature difference ΔT is a particularly important parameter in a convection experiment because it determines whether or not the fluid is in thermodynamic equilibrium. (It is precisely the fact that the nonequilibrium properties of the entire room can be described by a single parameter ΔT that constitutes the idealization of this experiment, and that motivated the extra experimental work of coating the floor and ceiling with copper.) If $\Delta T = 0$ so that the ceiling and floor have the same common temperature $T = T_1 = T_2$, then after some transient time, the air will be in thermodynamic equilibrium with zero velocity and the same uniform temperature T throughout. There is typically a transient time associated with approaching thermodynamic equilibrium because the air itself is rarely in such equilibrium without taking special precautions. For example, there might be a small breeze in the air when the door to the experimental room is closed or some part of the air may be a bit warmer than some other part because someone walked through the room. But as long as the room is sealed and the floor and ceiling have the same temperature, all macroscopic motion in the air will die out and the air will attain the same temperature everywhere.

As soon as the temperature difference ΔT becomes nonzero (with either sign), the air can no longer be in thermodynamic equilibrium since the temperature is spatially nonuniform. One says that the air is driven out of equilibrium by the

temperature difference since the nonequilibrium state is maintained as long as there is a temperature difference. For the case $\Delta T > 0$ of a warm floor and cool ceiling, as ΔT becomes larger and larger (but again held constant throughout any particular experiment), more and more energy flows through the air from the warm floor to the cooler ceiling, the system is driven further from equilibrium, and more and more complicated spatiotemporal dynamical states are observed. A temperature difference is not the only way to drive a system out of equilibrium as we will discuss in other parts of the book. Other possibilities include inducing relative motion (e.g. pushing water through a pipe which creates a shear flow), varying some parameter in a time-dependent fashion (e.g. shaking a cup of water up and down), applying an electrical current across an electrical circuit, maintaining one or more chemical gradients, or creating a deviation from a Maxwellian velocity distribution of particles in a fusion plasma.

For any particular mechanism such as a temperature difference that drives a system out of equilibrium, there are dissipative (friction-like) mechanisms that oppose this driving and act in such a way so as to restore the system to equilibrium. For the air convecting inside our room, there are two dissipative mechanisms that restore the air to a state of thermodynamic equilibrium if ΔT is set to zero. One is the viscosity of the fluid, which acts to decrease any spatial variation of the velocity field. Since it is known from fluid dynamics that the velocity of a fluid is zero at a material surface,[2] the only possible long-term behavior for a fluid approaching equilibrium in the presence of static walls is that the velocity field everywhere decays to zero. A second dissipative mechanism is heat conduction through the air. The warm regions of air lose heat to the cooler regions of air by molecular diffusion, and eventually the temperature becomes constant and uniform everywhere inside the room. These dissipative mechanisms of viscosity and heat conduction are always present, even when $\Delta T \neq 0$, and so one often talks about a sustained nonequilibrium system as a driven-dissipative system.

Rayleigh–Bénard convection is sometimes called buoyancy-induced convection for reasons that illustrate a bit further the driving and dissipative mechanisms competing in a nonequilibrium system. Let us consider an experiment in which the air in the room has reached thermal equilibrium with $\Delta T = 0$ and then the temperature difference ΔT is increased to some positive value. Small parcels of air near the floor will expand and so decrease in density as they absorb heat from the floor, while small parcels of air near the ceiling will contract in volume and increase in density as they lose heat to the ceiling. As illustrated in Fig. 1.2, buoyancy forces then appear that accelerate the lighter warmer fluid upwards and the heavier colder

[2] More precisely, the fluid velocity at a wall is zero in a frame of reference moving with the surface. Exercise 1.9 suggests a simple experiment using an electric fan to explore this point.

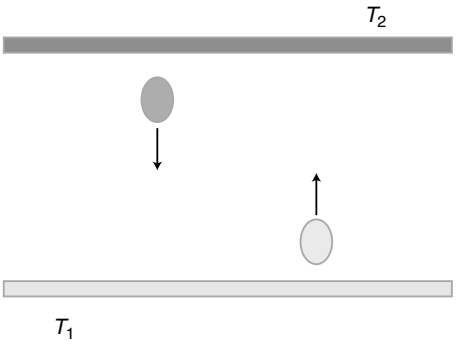

Fig. 1.2 Illustration of the driving and dissipative forces acting on small parcels of air near the floor and ceiling of the experimental room in Fig. 1.1 whose floor is warmer than its ceiling. The parcels are assumed to be small enough that their temperatures are approximately constant over their interiors. The acceleration of the parcels by buoyancy forces is opposed by a friction arising from the fluid viscosity and also by the diffusion of heat between warmer and cooler regions of the fluid. Only when the temperature difference $\Delta T = T_1 - T_2$ exceeds a finite critical value $\Delta T_c > 0$ can the buoyancy forces overcome the dissipation and convection currents form.

fluid downwards, in accord with the truism that "hot air rises" and "cold air falls." These buoyancy forces constitute the physical mechanism by which the temperature difference ΔT "drives" the air out of equilibrium. As a warm parcel moves upward, it has to push its way through the surrounding fluid and this motion is opposed by the dissipative friction force associated with fluid viscosity. Also, as the parcel rises, it loses heat by thermal conduction to the now cooler surrounding air, becomes more dense, and the buoyancy force is diminished. Similar dissipative effects act on a cool descending parcel.

From this microscopic picture, we can understand the experimental fact that making the temperature difference ΔT positive is a necessary but not sufficient condition for the air to start moving since the buoyancy forces may not be strong enough to overcome the dissipative effects of viscosity and conduction. Indeed, experiment and theory show that only when the temperature difference exceeds a threshold, a critical value we denote as ΔT_c, will the buoyancy forces be sufficiently large that the air will spontaneously start to move and a persistent spatiotemporal structure will appear in the form of convection currents. If the room's width L is large compared to its depth d so that the influence of the walls on the bulk fluid can be ignored, a precise criterion for the onset of convection can be stated in the form

$$R > R_c. \tag{1.1}$$

Table 1.1. *The isobaric coefficient of thermal expansion* α*, the kinematic viscosity* ν*, and the thermal diffusivity* κ *for air, water, and mercury at room temperature* $\mathrm{T} = 293\,\mathrm{K}$ *and at atmospheric pressure. These parameters vary weakly with temperature.*

Fluid	α (K^{-1})	ν $(\mathrm{m}^2/\mathrm{s})$	κ $(\mathrm{m}^2/\mathrm{s})$
Air	3×10^{-3}	2×10^{-5}	2×10^{-5}
Mercury	2×10^{-4}	1×10^{-7}	3×10^{-6}
Water	2×10^{-4}	1×10^{-6}	2×10^{-7}

The parameter R is defined in terms of various physical parameters

$$R = \frac{\alpha g d^3 \Delta T}{\nu \kappa}, \tag{1.2}$$

and the critical value of R has the approximate value

$$R_\mathrm{c} \approx 1708. \tag{1.3}$$

The parameters in Eq. (1.2) have the following meaning: g is the gravitational acceleration, about $9.8\,\mathrm{m/s^2}$ over much of the Earth's surface; $\alpha = -(1/\rho)(\partial\rho/\partial T)|_p$ is the fluid's coefficient of thermal expansion at constant pressure, and measures the relative change in density ρ as the temperature is varied; d is the uniform depth of the fluid; ΔT is the uniform temperature difference across the fluid layer; ν is the fluid's kinematic viscosity; and κ is the fluid's thermal diffusivity. Approximate values of the parameters α, ν, and κ for air, water, and mercury at room temperature ($T = 293\,\mathrm{K}$) and at atmospheric pressure are given in Table 1.1.

The combination of physical parameters in Eq. (1.2) is dimensionless and so has the same value no matter what physical units are used in any given experiment, e.g. System Internationale (SI), Centimeter-Gram-Seconds (CGS), or British. This combination is denoted by the symbol "R" and is called the Rayleigh number in honor of the physicist and applied mathematician Lord Rayleigh who, in 1916, was the first to identify its significance for determining the onset of convection. The pure number R_c is called the critical Rayleigh number R_c since it denotes the threshold that R must exceed for convection to commence. The value R_c can be calculated directly from the equations that govern the time evolution of a convecting fluid (the Boussinesq equations) as the criterion when the motionless conducting state of the fluid first becomes linearly unstable. The general method of this linear stability analysis is described in Chapter 2.

Despite its dependence on six parameters, you should think of the Rayleigh number R as simply being proportional to the temperature difference ΔT. The reason is that all the parameters in Eq. (1.2) except ΔT are approximately constant in a typical series of convection experiments. Thus the parameters α, ν, and κ in Eq. (1.1) depend weakly on temperature and are effectively fixed once a particular fluid is chosen. The acceleration g is fixed once a particular geographical location is selected for the experiment and the depth of the fluid d is typically fixed once the convection cell has been designed and is difficult to vary as an experimental parameter. Only the temperature difference ΔT is easily changed substantially and so this naturally becomes the experimental control parameter.

You should also note that the numerator $\alpha g d^3 \Delta T$ in Eq. (1.2) is related to quantities that determine the buoyancy force, while the denominator $\nu\kappa$ involves quantities related to the two dissipative mechanisms so Eq. (1.1) indeed states that instability will not occur until the driving is sufficiently strong compared to the dissipation. Most nonequilibrium systems have one or more such dimensionless parameters associated with them and these parameters are key quantities to identify and to measure when studying a nonequilibrium system.

What kind of dynamics can we expect for the air if the Rayleigh number R is held constant at some value larger than the critical value R_c? From Fig. 1.2, we expect the warm fluid near the floor to rise and the cool fluid near the ceiling to descend but the entire layer of ascending fluid near the floor cannot pass through the entire layer of descending fluid near the ceiling because the fluid is approximately incompressible. What is observed experimentally is pattern formation: the fluid spontaneously achieves a compromise such that some regions of fluid rise and neighboring regions descend, leading to the formation of a cellular convection "pattern" in the temperature, velocity, and pressure fields. The distance between adjacent rising and falling regions turns out to be about the depth of the air. Once the air begins to convect, the dynamics becomes too complicated to understand by casual arguments applied to small parcels of air and we need to turn to experiments to observe what happens and to a deeper mathematical analysis to understand the experimental results (see Figs. 1.14 and 1.15 below in Section 1.3.2). However, one last observation can be made. The motion of the fluid parcels inside the experimental system transport heat and thereby modify the temperature gradient that is felt in a particular location inside the system. Thus the motion of the medium changes the balance of driving and dissipation in different parts of the medium, and this is the reason why the dynamics is nonlinear and often difficult to understand.

The general points we learn from the above discussion about Rayleigh–Bénard convection are the following. There are mechanisms that can drive a system out of thermodynamic equilibrium, such as a flux of energy, momentum or matter through the system. This driving is opposed by one or more dissipative mechanisms such

as viscous friction, heat conduction, or electrical resistance that restore the system to thermal equilibrium. The relative strength of the driving and dissipative mechanisms can often be summarized in the form of one or more dimensionless parameters, e.g. the Rayleigh number R in the case of convection. Nonequilibrium systems often become unstable and develop an interesting spatiotemporal pattern when the dimensionless parameter exceeds some threshold, which we call the critical value of that parameter. What happens to a system when driven above this threshold is a complex and fascinating question which we look at visually in the next section and then discuss in much greater detail throughout the rest of the book. However, the origin of the complexity can be understood qualitatively from the fact that transport of energy and matter by different parts of the pattern locally modifies the balance of driving and dissipation, which in turn may change the pattern and the associated transport.

1.3 Examples of nonequilibrium patterns and dynamics

1.3.1 Natural patterns

In this section we discuss examples of pattern-forming nonequilibrium systems as found in nature while in the next section we look at prepared laboratory systems, such that a nonequilibrium system can be carefully prepared and controlled. These examples help to demonstrate the great variety of dynamics observed in pattern-forming nonequilibrium systems and provide concrete examples to keep in mind as we try to identify the interesting questions to ask.

We begin with phenomena at some of the largest length and time scales of the Universe and then descend to human length and time scales. An example of an interesting pattern on the grandest scales of the Universe is the recently measured organization of galaxies into sheets and voids shown in Fig. 1.3. Observation has shown that our Universe is everywhere expanding, with all faraway galaxies moving away from each other and from the Earth, and with the galaxies that are furthest away moving the fastest. The light from a galaxy that is moving away from Earth is Doppler-shifted to a longer wavelength (becomes more red) compared to the light coming from an identical but stationary galaxy. By measuring the extent to which known spectral lines are red-shifted, astronomers can estimate the recessional speed v of a galaxy and convert this speed to a distance d by using the so-called Hubble law $v = H_0 d$, where the Hubble constant H_0 has the approximate value $65\,\mathrm{km\,s^{-1}\,Mpc^{-1}}$ (and a megaparsec Mpc is about 3×10^{19} km or about 3×10^6 light years).

Figure 1.3 summarizes such distance measurements for about 100 000 galaxies out to the rather extraordinary distance of about four billion light years which is

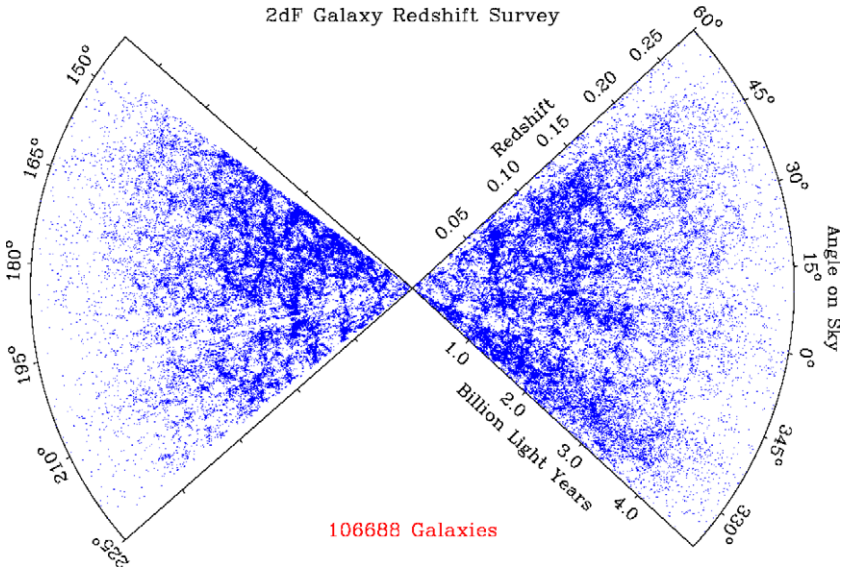

Fig. 1.3 Spatial distribution of 106 688 galaxies as measured in the 2dF (Two-degree Field) Galaxy Redshift survey out to a depth of over 4 billion light years from Earth. The left and right halves represent investigations over two separate arcs of the sky; the angles indicate astronomical declination, which is the angular latitude of a celestial object north or south of the celestial equator. Each point represents a galaxy whose distance from Earth is indicated in billions of light years or equivalently in terms of its redshift $z = \Delta\lambda/\lambda = v/c$ of the galaxy's light spectrum, where v is the velocity of recession from Earth. The distribution of galaxies is a nonuniform fractal-like structure with huge voids and walls.

comparable to the size of the Universe itself. Rather surprisingly, the galaxies do not fill space uniformly like molecules in a gas but instead are clustered in sheets and walls with large voids (relatively empty regions of space) between them. Here the pattern is not a geometric structure (e.g. a lattice) but a statistical deviation from randomly and uniformly distributed points that is difficult for the human visual system to quantify. Perhaps the closest earthly analogy would be a foam of bubbles in which the galaxies are concentrated on the surfaces of the bubbles. The reason for this galactic structure is not known at this time but is presumably a consequence of the details of the Big Bang (when matter first formed), the expansion of the Uuniverse, the effects of gravity, and the effects of the mysterious dark matter that makes up most of the mass of the Universe but which has not yet been directly observed or identified.

A second example of grand pattern formation is the M74 galaxy shown in Fig. 1.4. Now a galaxy consists of a huge number of about 10^{10} stars and has a net angular momentum from the way it was born by the condensation of a large hydrogen cloud.

Fig. 1.4 Photograph of the M74 spiral galaxy, a gravitationally bound island of 100 billion stars, approximately 100 000 light years wide, that lies about 35 000 000 light years from Earth in the Pisces constellation. Why galaxies form in the first place and why they appear in spiral, elliptical, and irregular forms remains incompletely understood. (Gemini Observatory, GMOS team.)

From just these facts, you might expect galaxies to be rotating featureless blobs of stars with a mass density that varies monotonically as a function of radius from the center. Such blobs do in fact exist and are known as elliptical galaxies. However many galaxies do have a nonuniform mass density in the form of two or more spiral arms as shown in Fig. 1.4. Our own galaxy, the Milky Way, is such a spiral galaxy and our Solar System lives in one of its high-density spiral arms.

Why galaxies evolve to form spiral arms is poorly understood and is an important open question in current astrophysical research. As we will see in the next section and in Chapter 11, laboratory experiments show that spiral formation is common for nonequilibrium media that have a tendency to oscillate in time or that support wave propagation. Further, experiments show that a tendency to form spirals is insensitive to details of the medium supporting the spiral. So a galactic spiral may not be too surprising since there are mechanisms in galaxies that can produce wave propagation. For example, some researchers have proposed that the spiral arms are detonation waves of star formation that propagate through the galaxy, somewhat analogous to the excitation waves observed in the Belousov–Zhabotinsky reaction–diffusion system shown below in Fig. 1.18 and discussed later in Chapter 11. Some interesting questions to ask about Fig. 1.4 are what determines the frequency of rotation of the spiral arms (which is not the same as the orbital rotation rate of the matter within a spiral arm) and what determines the spiral pitch (how tightly the spiral is wound)?

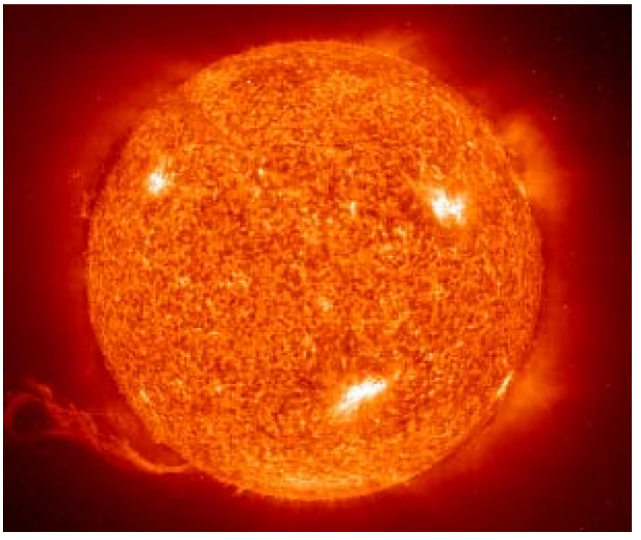

Fig. 1.5 Photograph of the Sun's surface in ultraviolet light, showing a complex time-dependent granular structure. The small bright regions are granules approximately 1000 km across (the Sun itself is about 100 Earth diameters in size) and correspond to hot plasma rising from the interior while the darker borders of the granules correspond to cooler plasma descending back to the interior. The filamentary structure exuding from the surface are plasma filaments following magnetic field lines.

Figure 1.5 descends from the scale of a galaxy to that of a star and shows a snapshot of the ultraviolet light emitted from the highly turbulent plasma in the so-called photosphere of the Sun. Heat diffuses by collisions from the Sun's small dense and extremely hot core (20 million degrees Kelvin) out to about two-thirds of the radius of the Sun, at which point the heat is transported to the cooler surface (about 6000 K) by convective motion of the Sun's plasma. The small bright dots in Fig. 1.5 are 1000 km-sized features called "granules" and correspond to the top of convection cells, the darker boundaries are where the cooler plasma descends back into the interior. The Rayleigh number R in Eq. (1.1) can be estimated for this convecting plasma and turns out to have the huge value of 10^{12} so Fig. 1.5 represents a very strongly driven nonequilibrium system indeed.

Figure 1.5 and related movies of the Sun's surface suggest many interesting questions related to pattern formation, many of which are not yet answered. One question is that of what determines the distributions of the sizes and lifetimes of the granules. Another question is that of how any organized structure persists at all since, at any given point, the plasma is varying rapidly and chaotically. Other solar images show that the smallest granules are found to cluster together to form convective structures called super-granules which may be 30 times larger on average. Why

does this happen and what determines this new length scale? And what is the role of the magnetic field in all of this? Unlike the convecting air in Fig. 1.1, the Sun's plasma is a highly conducting electrical medium and its motion is influenced by the Sun's magnetic field (by a Lorentz force acting on currents in the plasma) and the magnetic field in turn is modified by the motion of the plasma (by Ampère's law, since currents generate a magnetic field). The magnetic field is known to be especially important for understanding the occurrence of sunspots, whose number varies approximately periodically with a 22-year cycle. There is evidence that the Earth's climate is partly influenced by the average number of sunspots and so a full understanding of the weather may require a deeper understanding of the Sun's spatiotemporal dynamics.

Our next example of pattern formation should be familiar to readers who have followed the observations of the planet Jupiter by the Voyager spacecraft and by the Hubble Space Telescope. Figure 1.6 shows a photograph of Jupiter in which one can see a nonequilibrium striped pattern that is common to all of the gas giants (Jupiter, Saturn, Neptune, and Uranus). Careful observation of the bands and of their dynamics shows that they are highly turbulent time-dependent flows of the outer portion of Jupiter's atmosphere, with adjacent bands flowing in opposite directions with respect to Jupiter's axis of rotation. Again numerous questions suggest themselves such as why do the bands form, what determines their wavelength of approximate

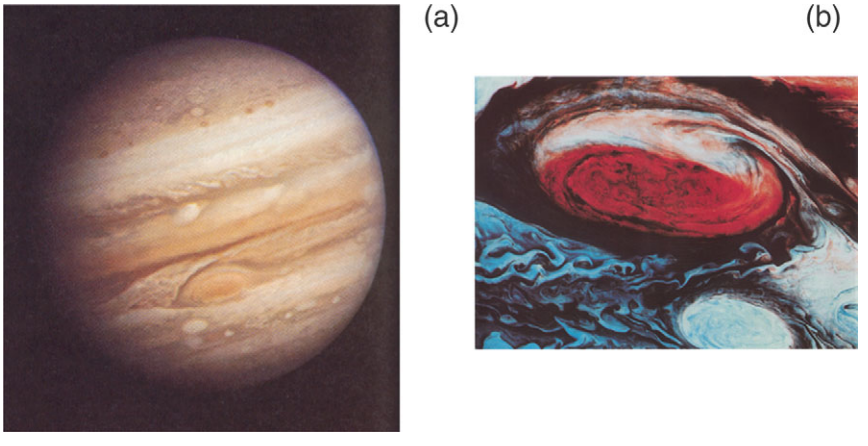

Fig. 1.6 (a) Photograph of the planet Jupiter (about 11 Earth diameters in size), showing a colored banded nonequilibrium structure. Such bands and spots are common to all the outer gaseous planets and arise from convection together with shear flow driven by the planet's rotation. (b) Blow-up of the famous great Red Spot, which is about the same size as the Earth. The persistence over many centuries of this turbulent spot within the surrounding turbulent atmosphere remains an intriguing mystery.

periodicity (their spacing is fairly uniform across the planet), and how do such bands survive in such a highly fluctuating fluid medium? The Red Spot and other similar spots pose a problem of their own, namely how do such large localized features (which are themselves time-dependent and strongly turbulent) survive in the middle of such a strongly fluctuating time-dependent fluid? The Red Spot was first observed by Galileo in the 1500s and so has been a persistent feature for at least 500 years.

The mechanisms that drive these nonequilibrium stripes and spots are not hard to identify. Jupiter's core is known to be hot and the transport of heat from the core out through its atmosphere causes convection in the outermost layer, just as in Fig. 1.1. However, the convection is substantially modified by Jupiter's rapid rotation around its axis, about once every 10 hours. As warm and cold parcels of fluid rise and descend, they are pushed to the side by large Coriolis forces and so follow a spiraling path.

We next turn to terrestrial examples of natural pattern formation and dynamics. While visiting a beach or desert, you have likely seen nonequilibrium pattern formation in the form of approximately periodic ripples found in sand dunes or sand bars, an example of which is shown in Fig. 1.7(a). The driven-dissipative nature of sand ripples is readily understood although the particular details of this pattern formation are not. The driving comes from wind (or water) flowing over the sand. When moving fast enough, the wind lifts sand grains into the air, transferring translational and rotational energy to them. These grains eventually fall back to earth and dissipate their energy into heat by friction as they roll and rub against other sand grains. The formation of nearly regular stripes is understood in rough outline, both from laboratory experiments and from computer simulations that can track the motion of tens of thousands of mathematical grains that collide according to specified rules. One surprise that came out of studying the stripes in sand dunes is that there is not a well-defined average wavelength as is the case for a convection pattern, for which the average wavelength is determined simply by the depth of the fluid. Instead, the average wavelength grows slowly with time, and can achieve kilometer length scales as shown in the Martian sand dunes of Fig. 1.7(b).

Another familiar and famous terrestrial example of pattern formation is a snowflake (see Fig. 1.8). This is a nonequilibrium system rather different than any described so far in that the pattern is formed by crystalline dendrites (these are the needle-like branches of a snowflake) that grow into the surrounding air. Unlike a convecting fluid in a fixed geometric box, the dendrite's shape itself changes as the system evolves. The nonequilibrium driving for snowflake formation is the presence of air that is supersaturated with water vapor. (In contrast, an equilibrium state would involve a static ice crystal in contact with saturated water vapor.) Each tip of the snowflake grows by adsorbing water molecules onto its surface from the

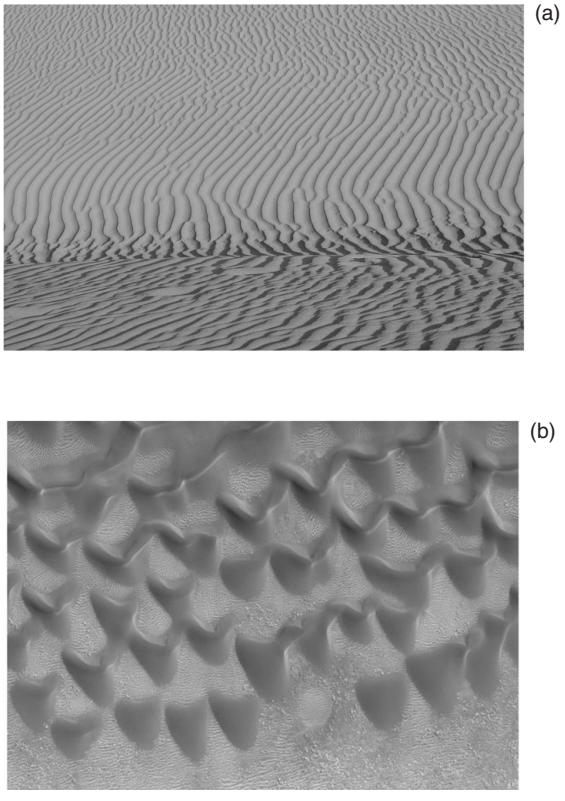

Fig. 1.7 (a) Pattern formation in wind-swept sand at the Mesquite Flat Sand Dunes in Death Valley, California. The ripple spacing is about 10 cm. The foreground of the picture is the top of a dune, and the remainder shows ripples on the valley floor. (Photo by M. C. Cross.) (b) Sand dunes in the Proctor Crater on Mars, as taken by the Mars Global Surveyor spacecraft in September of 2000 (Malin Space Science Systems). The average distance between dune peaks is about 500 m.

surrounding air, and the rate at which the tip grows and its shape are determined in a complex way by how rapidly water molecules in the surrounding air can diffuse to the crystalline tip, and by how rapidly the heat released by adsorption can be dissipated by diffusion within the air.

There are many fascinating questions associated with how snowflakes form. For example, what determines the propagation speed of the tip of a dendrite and is there a unique speed for fixed external conditions? Is there a unique shape to the tip of a dendrite and on what details does this shape depend? Why are the arms of a snowflake approximately the same length and have approximately the same intricate shape but are not exactly identical? And what causes the formation of the side-branches, whose rich spatial structure is such that no two snowflakes are presumably ever alike? Scientists have made progress over the last twenty years in

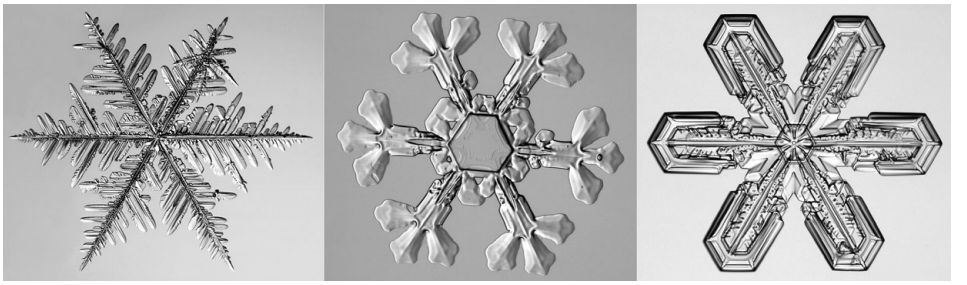

Fig. 1.8 Photographs by Kenneth Libbrecht of three snowflakes. The overall hexagonal symmetry reflects the underlying crystalline structure of water molecules while the intricate structure of the similar but not identical branches is a consequence of the instability of the dendritic tips, which propagate at an approximately constant speed into the surrounding supersaturated water vapor. (Photos courtesy of Kenneth Libbrecht.)

answering many of these questions. As a result of this progress, snowflakes rank among the best understood of all nonequilibrium systems.

Beyond their aesthetic beauty, you should appreciate that snowflakes belong to a technologically valuable class of nonequilibrium phenomena involving the synthesis of crystals and alloys. An example is the creation of meter-sized ultra-pure single crystal boules of silicon from which computer chips are made. One way to create such an ultra-pure boule is to pull a crystal slowly out of a rotating and convecting liquid silicon melt. In such a process, scientists and engineers have found that they need to understand the instabilities and dynamics of the solid–liquid interface (called a solidification front) since the extent to which undesired impurities can be prevented from diffusing into and contaminating the crystal depends delicately on the dynamics of the front. The metals that are the fabric of our modern world are also usually formed by solidification from the melt. Their strength, flexibility, and ductility are largely determined by the size and intermingling of small crystalline grains rather than by the properties of the ideal crystal lattice. This microstructure depends sensitively on the nonequilibrium growth process, for example how the solidification fronts propagate from the many nucleation sites. The tip of a snowflake dendrite is also a solidification front (although now between a solid and gas) and basic research on snowflakes has provided valuable insights for these other more difficult technological problems.

We turn finally to two examples of biological natural patterns and dynamics. A heroine of biological pattern formation is the slime mold *Dictyostelium discoideum*, which is a colony of tiny amoeba-like creatures – each about 10 microns in size – that live on forest floors. These cells spend most of their lives as solitary creatures foraging for food but when food becomes scarce, the cells secrete an attractant (cyclic AMP) into their environment that triggers pattern formation and the eventual

aggregation of about 10^5 cells into a central mass. (This mass later evolves into a multicellular structure that can distribute cells to new regions where resources may be available, but that is another story.) Of interest to us is the spontaneous spatiotemporal pattern of propagating spiral waves of cells that is observed in the early stages of aggregation (Fig. 1.9). This pattern turns out to be remarkably similar to that observed in carefully prepared reacting and diffusing inorganic reagents (see Fig. 1.18(a) below), and you will indeed learn later in Chapter 11 that such multi-spiral states are observed in many nonequilibrium media and that many details of such states are understood theoretically.

Experiment and theory have shown that, in rough outline, the slime-mold pattern arises from a nonlinear dynamics in which cells secrete an attractant, cells move toward higher concentrations of the attractant (a process known as chemotaxis), and attractant is destroyed by secretion of an appropriate enzyme. The slime-mold dynamics is nonequilibrium because there are sustained chemical gradients; temperature and velocity gradients are not important here as they were for a convecting flow. Figure 1.9 suggests some quantitative questions similar to those suggested by Fig. 1.4, namely what determines the frequency and velocity of the waves in the spirals and how do these quantities vary with parameters? And biologists would like to know why slime molds use this particular spatiotemporal pattern to self-organize into a new multicellular structure.

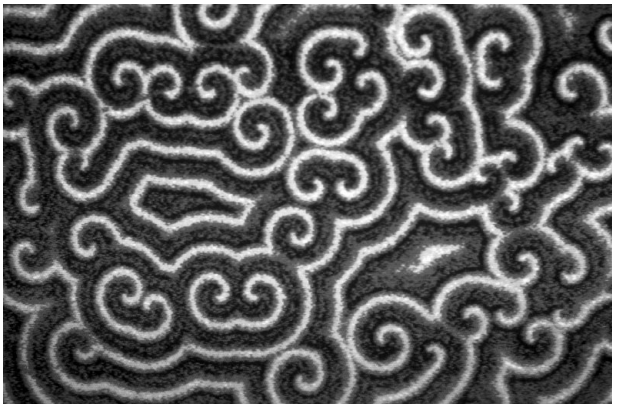

Fig. 1.9 Photograph of a starving slime-mold colony in the early stages of aggregation. The cells were placed on an 8-cm-wide caffeine-laced agar dish with an average density of 106 cells/cm^2. The field of view covers 4 cm. The light regions correspond to elongated cells that are moving with a speed of about 10 microns/minute by chemotaxis toward higher secretant concentrations. The dark regions correspond to flattened cells that are stationary. The spiral waves rotate with a period of about 5 minutes. This early aggregation stage persists for about four hours after which the pattern and cell behavior changes substantially, forming thread-like streams. (Figure courtesy of Dr. Florian Siegert.)

Our second biological example of a natural pattern formation is the important medical problem of ventricular fibrillation. This occurs when the thick muscle tissue surrounding the left ventricle (the largest of the four heart chambers) enters into an irregular spatiotemporal electrical state that is no longer under the control of the heart's pacemaker (the sinoatrial node). In this fibrillating state, the ventricular muscle cannot contract coherently to pump blood, and the heart and the rest of the body start to die from lack of oxygen. A common but not always successful treatment is to apply a massive electrical current to the heart (via a defibrillator) that somehow eliminates the irregular electrical waves in the left ventricle and that resets the heart tissue so that the ventricle can respond once again to the sinoatrial node.

Why the dynamics of the left ventricular muscle sometimes changes from periodic coherent contractions to a higher-frequency nonperiodic incoherent quivering is still poorly understood. One intriguing observation is that ventricular fibrillation is observed primarily in mammals whose hearts are sufficiently large or thick. Thus mice, shrews, and guinea pigs do not easily suffer ventricular fibrillation while pigs, dogs, horses, and humans do. Experiments, theory, and simulations have begun to provide valuable insights about the spatiotemporal dynamics of ventricular fibrillation and how it depends on a heart's size and shape, as well as on its electrical, chemical, and mechanical properties. An example is Fig. 1.10, taken

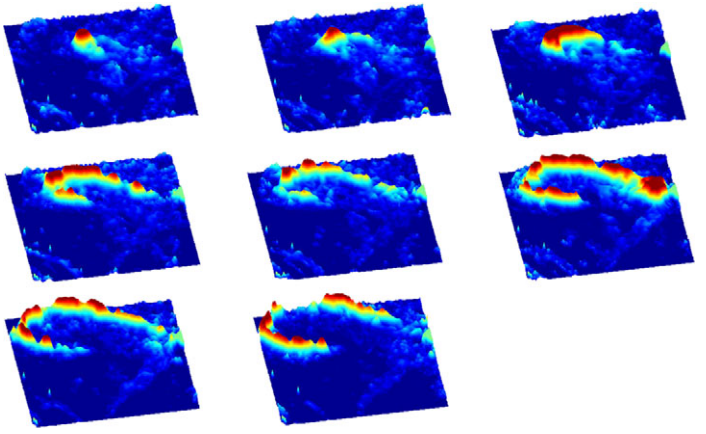

Fig. 1.10 Visualization of the surface voltage potential of an isolated blood-perfused dog heart in a fibrillating state. The surface of the left ventricle was painted with a dye whose fluorescent properties are sensitive to the local transmembrane voltage (which is of order 80 millivolts), and then the fluorescence under a strong external light source was recorded as a function of time. The waves propagate at a speed of about 20–40 cm/s (heart tissue is anisotropic and the speed varies with the direction of propagation), a range that is about the same for most mammalian hearts. (From Witkowski *et al.* [114].)

from a pioneering experiment that visualized the time-dependent voltage pattern on the surface of a fibrillating dog heart. This electrical pattern is complex and consists of spiral-like waves that move around, and that sometimes terminate or are created through collisions with other waves. Since muscle tissue contracts shortly after an electrical wave front passes through it, the irregular geometric shape of the waves in Fig. 1.10 explains directly why the heart is not contracting coherently and so has difficulty pumping blood. The similarity of the dynamics to that observed in slime molds and in reacting and diffusing chemical solutions is likely misleading. Left ventricular muscle is a rather thick three-dimensional nonequilibrium medium and recent theoretical research suggests that the surface patterns in Fig. 1.10 are likely intersections by the surface of more intricate three-dimensional electrical waves inside the heart wall that experimentalists have not yet been able to observe directly.

Given that ventricular fibrillation kills over 200 000 people in the United States each year and is a leading cause of death in industrial countries worldwide, understanding the onset and properties of ventricular fibrillation and finding ways to prevent it remain major medical and scientific goals. Chapter 11 will discuss heart dynamics in more detail since it turns out to be one of the more exciting current frontiers of nonequilibrium pattern formation and illustrates well many of the concepts discussed in earlier chapters.

1.3.2 Prepared patterns

The previous section surveyed some of the patterns and dynamics that are observed in natural nonequilibrium systems. For the most part, these natural systems are difficult to study and to understand. Unlike the idealized room of convecting air in Fig. 1.1, natural systems are often inhomogeneous and so difficult to characterize, they are subject to many different and simultaneous mechanisms of driving and dissipation (some of which are not known or are not well understood), and some systems are simply too remote or too big for direct experimental investigation. In this section, we survey some nonequilibrium phenomena observed in idealized carefully controlled laboratory experiments and reach the important conclusion that even such highly simplified systems can produce a dazzling variety of complex patterns and dynamics, often with properties similar to those observed in natural systems.

Figure 1.11 shows several patterns and dynamical states in a Taylor–Couette fluid dynamics experiment. The experiment is named after the French scientist Maurice Couette who, in the late 1800s, was one of the first to use this apparatus to study the shearing of a fluid, and after the British scientist Geoffrey Taylor who used this system in the early 1920s to make the first quantitative comparison in fluid dynamics of a linear stability analysis with experiment (see Figs. 2.5 and 2.6 in Section 2.4).

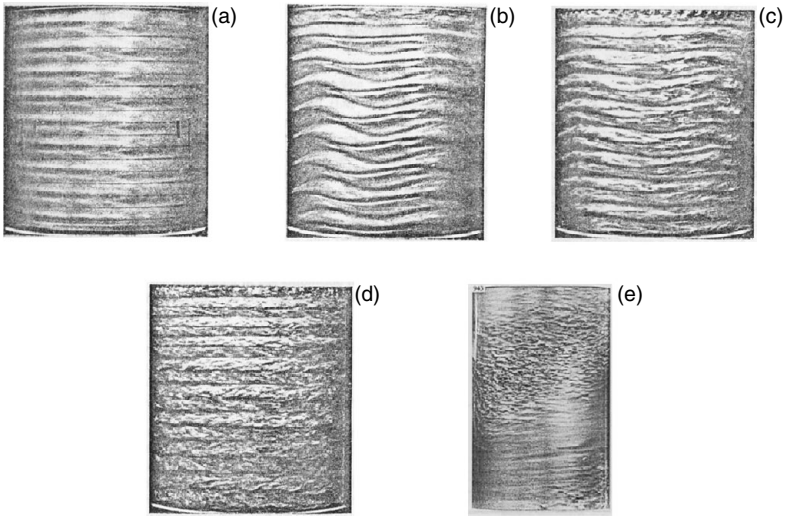

Fig. 1.11 Five examples of pattern formation in a Taylor–Couette fluid dynamics experiment, in which a fluid filling the thin annular gap between two concentric cylinders is sheared by rotating the inner and outer cylinders at constant but different speeds. The flow pattern was visualized by shining light through the transparent outer cylinder and scattering the light off a low concentration of shiny impurities such as aluminum flakes. In panels (a)–(d), the outer cylinder is at rest, while the inner cylinder is rotating at different angular frequencies corresponding respectively to inner Reynolds numbers of $\mathcal{R}_i/\mathcal{R}_c = 1.1$, 6.0, 16.0, and 26.5, where $\mathcal{R}_c$ is the critical value at which laminar flow becomes unstable to Taylor cells. The fluid is water at $T = 27.5\,^\circ$C with kinematic viscosity $\nu = 8.5 \times 10^{-7}\mathrm{m}^2/\mathrm{s}$. The height of the two glass cylinders is $H = 6.3$ cm while the outer and inner radii are respectively $r_2 = 2.54$ cm and $r_1 = 2.22$ cm. Only pattern (a) is time-independent. (e) A so-called stripe-turbulent state found in a different Couette experiment with parameters $r_1 = 5.3$ cm, $r_2 = 5.95$ cm, and $H = 20.9$ cm. The inner and outer Reynolds numbers are $\mathcal{R}_i = 943$ and $\mathcal{R}_o = -3000$. (Panels (a)–(d) from Fenstermacher *et al*. [35]; panel (e) from Andereck *et al*. [3].)

Taylor–Couette flow has some similarities to Rayleigh–Bénard convection in that a fluid like water or air is placed between two walls, here the inner and outer boundaries of two concentric cylinders (with the outer cylinder usually made of glass to facilitate visualization). But instead of being driven out of equilibrium by a temperature gradient, the fluid is driven out of equilibrium by a velocity gradient that is sustained by using motors and gears to rotate the inner and outer cylinders at constant angular frequencies ω_i and ω_o respectively (not necessarily with the same sign). The fluid temperature is constant throughout.

As was the case for convection, a dimensionless combination of system parameters can be identified as the "stress" parameter that measures the strength of driving compared to dissipation. When both cylinders are spinning, there are two such parameters and they are traditionally called the inner and outer Reynolds numbers.

They have the form

$$\mathcal{R}_{\rm i} = \frac{\omega_{\rm i} r_{\rm i}(r_{\rm o} - r_{\rm i})}{\nu}, \quad \mathcal{R}_{\rm o} = \frac{\omega_{\rm o} r_{\rm o}(r_{\rm o} - r_{\rm i})}{\nu}, \tag{1.4}$$

where $r_{\rm i}$ is the radius of the outer wall of the inner cylinder, $r_{\rm o}$ is the radius of the inner wall of the outer cylinder, and ν is again the fluid's kinematic viscosity. Note that there are many other valid ways to define dimensionless stress parameters here, e.g. for an inner stress parameter the combinations $\omega_{\rm i} r_{\rm i}^2/\nu$, $\omega_{\rm i}(r_{\rm o}^2 - r_{\rm i}^2)/\nu$, or even $(1/2)\omega_{\rm i}^2(r_{\rm o}+r_{\rm i})(r_{\rm o}-r_{\rm i})^3/\nu^2$ could be used instead. (This last combination is called the Taylor number and is basically the square of a Reynolds number.) Often the appropriate choice of a stress parameter is suggested by a linear stability analysis of the dynamical equations but in some cases the choice is simply set by historical precedent.

Let us consider first the situation of a fixed outer cylinder so that $\omega_{\rm o} = 0$ and $\mathcal{R}_{\rm o} = 0$. Then experiments show – in agreement with theory – that the velocity field $\mathbf{v}$ of the fluid is time-independent and featureless[3] until the inner Reynolds number $\mathcal{R}_{\rm i}$ exceeds a critical value $\mathcal{R}_{\rm c} \approx 100$. (The specific value of $\mathcal{R}_{\rm c}$ depends on the ratio of radii $r_{\rm o}/r_{\rm i}$ and on the height of the cylinders.) For $\mathcal{R} > \mathcal{R}_{\rm c}$, interesting patterns appear and these can be visualized by doping the fluid with a small concentration of metallic or plastic flakes that reflect external light. Unlike the natural systems described in the previous section, a Taylor–Couette cell can be accurately controlled with the temperature, inner and outer radii, and rotational velocities all determined to a relative accuracy of 1% or better. The results of such experiments are highly reproducible and so the response of the system to small changes in the parameters can be carefully and thoroughly mapped out.

Figure 1.11 shows examples of the patterns observed in particular Taylor–Couette cells of fixed fluid, height, and inner and outer radii, for different constant values of the Reynolds numbers $\mathcal{R}_{\rm i}$ and $\mathcal{R}_{\rm o}$. For $\mathcal{R}_{\rm o} = 0$ and $\mathcal{R}_{\rm i} > \mathcal{R}_{\rm c}$ just larger than the critical value $\mathcal{R}_{\rm c}$ at which a uniform state becomes unstable, Fig. 1.11(a) shows that the fluid spontaneously forms a time-independent pattern of uniformly spaced azimuthally symmetric donut-like cells called Taylor cells. Given the static one-dimensional nature of this pattern, there is really only one interesting question to ask, which is the question of wave number selection: what determines the wavelength of the Taylor cells and is this wavelength unique for fixed external parameters? This is a basic question in pattern formation, and we will return to it a number of times in this book.

As the inner Reynolds number $\mathcal{R}_{\rm i}$ is increased further, the static Taylor cells become unstable to a time-periodic state consisting of waves that propagate around

[3] "Featureless" here means that the velocity field $\mathbf{v}$ is independent of the azimuthal and axial coordinates and has a simple monotonic dependence on the radial coordinate.

each Taylor cell. Such a transition in a dynamical system is often called a bifurcation.[4] This regime is called the wavy vortex state, a snapshot of which is shown in Fig. 1.11(b). The angular frequency of the waves is somewhat less than the rotational frequency of the inner cylinder and is known experimentally to depend on the values of the parameters r_o, r_i, and ν. For still larger $\mathcal{R}_i$, a second Hopf bifurcation takes place, leading to time-quasiperiodic dynamics and a more complex spatial motion known as the modulated wavy vortex state (see Fig. 1.11(c)). For still larger values of $\mathcal{R}_i$ (see Fig. 1.11(d)), the fluid becomes turbulent in that the time dependence is everywhere nonperiodic, there is no longer any identifiable wave motion, and the spatial structure is disordered. Note how one can perceive the ghostly remains of the Taylor cells in this turbulent regime, raising again a question similar to the one we asked about the Red Spot of Jupiter, namely how can some kind of average structure persist in the presence of strong local fluctuations? (A theoretical understanding of this strongly driven regime has not yet been developed.) A practical engineering question to answer would be to predict the average torque on the inner cylinder as a function of the Reynolds number $\mathcal{R}$. How does the complex fluid motion modify the resistance felt by the motor, which is turning the inner cylinder at constant speed?

Figure 1.12 summarizes many of the dynamical states that have been discovered experimentally in Taylor–Couette flows for different values of the inner and outer Reynolds numbers.[5] This figure raises many interesting questions. Where do all these different states come from and are these the only ones that can occur? Is the transition from one state to another, say from Couette flow to Taylor vortex flow or from spiral turbulence to featureless turbulence, similar to an equilibrium phase transition corresponding to the melting of a crystal to form a liquid or the evaporation of a liquid to form a gas? Little is known about most of these states and their transitions. One of the few theoretical successes is the heavy black line, which Taylor predicted in 1923 as the boundary separating the featureless laminar regime of Couette flow from various patterned states.

While quite interesting, the patterns in Taylor–Couette flows tend to have mainly a one-dimensional cellular structure and so we turn next to laboratory experiments of Rayleigh–Bénard convection that show two- and three-dimensional pattern formation and dynamics. As you learn by answering Exercise 1.5, a room like that described in Fig. 1.1 is impractical for convection experiments because the onset of convection is reached for a tiny difficult-to-achieve temperature difference, and the

[4] A bifurcation of a dynamical system that introduces an intrinsic temporal oscillation is called a Hopf bifurcation, so the transition of Taylor cells to the wavy vortex state in Fig. 1.11(b) is a spatiotemporal example of a Hopf bifurcation.

[5] This diagram is not complete since some regimes are hysteretic. One can then observe different states for the same values of $\mathcal{R}_i$ and $\mathcal{R}_o$, depending on the history of the experiment.

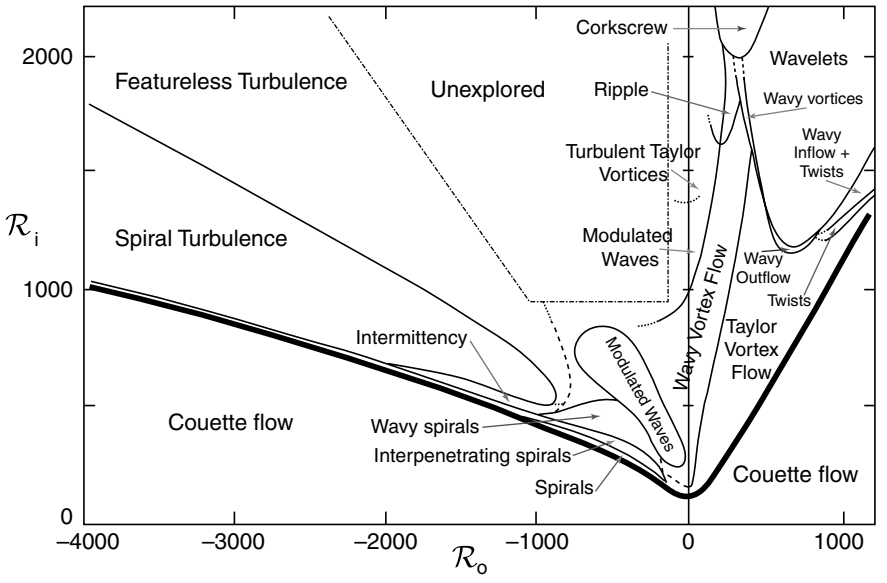

Fig. 1.12 Phase diagram of patterns observed in Taylor–Couette flow as a function of the inner Reynolds number $\mathcal{R}_i$ and the outer Reynolds number $\mathcal{R}_o$. The heavy line denotes the boundary between featureless flow below the line and patterned states above the line. (Redrawn from Andereck *et al*. [3].)

time scales for observation are uncomfortably long. Instead, experimentalists use tiny convection cells that are Swiss watches of high precision, with a fluid depth of perhaps $d \approx 1\,\text{mm}$ and a width $L \approx 5\,\text{cm}$. The bottom and top plates of such apparatuses are machined and polished to be flat to better than one micron and then aligned to be parallel to better than one part in 10^4. The bottom plate may be made of gold-plated copper which has a thermal conductivity about 1000 times higher than water or air. The upper plate is often made of a thin, wide (and expensive!) sapphire plate, which has the nice properties of being optically transparent (allowing visualization of the flow) and of being an excellent thermal conductor. The mean temperature of the fluid and the temperature difference ΔT across the plates can be controlled to better than 1 milliKelvin (again about one part in 10^4) for more than a month of observation at a time. A Rayleigh–Bénard convection experiment has a significant advantage over Taylor–Couette and other fluid experiments in having no moving parts in contact with the fluid. Thus motors or pumps that oscillate and vibrate can be avoided and the observed dynamics of the convecting fluid is intrinsic since the fluid is bounded by time-independent spatially homogeneous boundaries.

The patterns of a convecting flow are usually visualized by a method called shadowgraphy (Fig. 1.13). The index of refraction of a fluid is weakly dependent

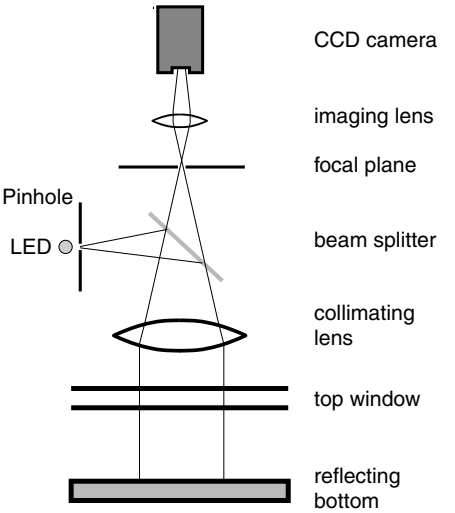

Fig. 1.13 Schematic drawing of the shadowgraphy method for visualizing a Rayleigh–Bénard convection pattern. Monochromatic light from a light emitting diode (LED) is reflected by a beam splitter through the transparent top plate (often made of sapphire) of the convection experiment. The light beams are refracted by the warm and cold regions of the fluid which act as diverging and converging lenses respectively. The light is then reflected off the mirror bottom plate, is refracted once more through the convection rolls, back through the beam splitter, and is then analyzed by a CCD (charge-coupled-device) videocamera. (From deBruyn *et al*. [30].)

on temperature so that the warm rising plumes of fluid act as a diverging lens and the cold descending plumes of fluid act as a converging lens. A parallel beam of light passing through the convecting fluid will be refracted by the convection rolls, and focused toward the regions of higher refractive index. The convection rolls act as an array of lenses producing, at the imaging plane, a pattern of alternating bright and dark regions, with the bright regions corresponding to the cold down-flow and the dark regions corresponding to the warm up-flow. These images are often sufficient to identify the interesting patterns and their dynamics, and can be recorded by a video camera and stored in digital form for later analysis.

Given this background, you can now appreciate the experimental data of Fig. 1.14, which shows three convection patterns in large cylindrical geometries. As we will see, the typical size of the structures in the convecting flow is set by the depth of the layer of fluid. The important parameter describing the "size" of the experimental system is therefore the aspect ratio defined as the lateral extent of the convecting fluid (e.g. the radius of a cylindrical cell) divided by the fluid depth. We will use the symbol Γ for the aspect ratio. The convecting

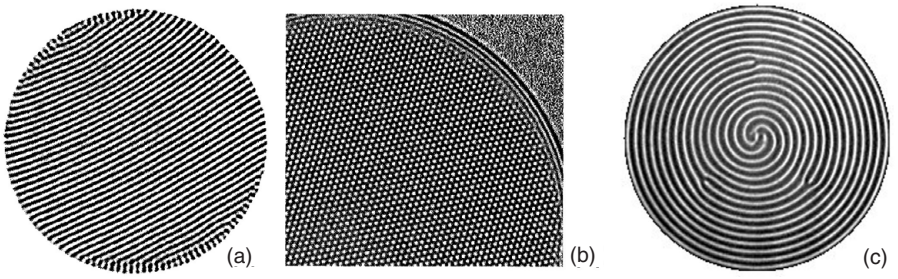

Fig. 1.14 Visualization of convecting fluid patterns in large cylindrical cells by the shadowgraphy method of Fig. 1.13. The white regions correspond to descending colder fluid and the dark stripes to rising warmer fluid. (a) A stationary stripe pattern just above onset for $R = 1.04R_c$, with a local wavelength that is close to twice the depth of the fluid. This cell has an aspect ratio of $\Gamma = r/d = 41$. (b) A remarkably uniform stationary lattice of hexagonal convection cells is found in gaseous CO_2 for $R = 1.06R_c$. Here the fluid is descending in the middle of each hexagonal cell and rising along its boundaries. Only a portion of an aspect-ratio $\Gamma = 86$ cell is shown. With a small increase in the Rayleigh number to $R = 1.15R_c$, the hexagonal cells in (b) change into a slowly-rotating spiral. A three-armed spiral pattern is shown in (c). (Panels (a) and (b) from deBruyn *et al.* [30]; (c) from the website of Eberhard Bodenschatz.)

fluid in the experiments shown in Fig. 1.14 is compressed carbon dioxide at room temperature.

Figure 1.14(a) shows a most remarkable fact. After some transient dynamics not shown, the rising and falling plumes of fluid self-organize into a time-independent periodic lattice of straight lines, often called "stripes." The surprise is that the circular geometry of the surrounding walls has little effect on this final geometric pattern; one might have expected instead the formation of axisymmetric (circular) convection rolls with the same symmetry as that of the lateral walls.

Under slightly different conditions Fig. 1.14(b) shows that a nearly perfect time-independent lattice of hexagonal convection cells forms. In each hexagon, warm fluid rises through its center and descends at its six sides, and the diameter of each hexagon is about the depth of the fluid. As was the case for the stripe pattern, the cylindrical shape of the lateral walls seems to have little effect on the pattern formation within the fluid except for the few cells directly adjacent to the lateral wall.

In Fig. 1.11(b) and in Figs. 1.14(a) and (b), we seem to be observing an intrinsic ordering of the convection cells which you might guess is analogous to the formation of a crystalline lattice of atoms as some liquid is slowly cooled. However, as we discuss in the next chapter and later in the book, the mechanism for formation of stationary nonequilibrium periodic lattices is fundamentally different than the mechanism by which periodic equilibrium crystalline lattices form, e.g. the cubic

lattice of sodium and chlorine atoms in table salt. In the latter case, atoms attract each other at long distances and repel each other at short distances so that the lattice spacing is determined by the unique energy minimum for which the repulsive and attractive forces balance. In contrast, the lattice spacing in a nonequilibrium system is determined by dynamic mechanisms that have nothing to do with repulsion or attraction and with which no energy-like quantity can generally be associated. A consequence is that nonequilibrium lattices may lack a unique lattice spacing for specified experimental conditions.

For the same fluid and geometry of Fig. 1.14(b), if the Rayleigh number is increased just a tiny bit more to the value $R = 1.15R_c$, the hexagonal lattice disappears and is replaced by a large slowly rotating spiral. A similar spiral pattern in a smaller aspect ratio cell is shown in Fig. 1.14(c). If you look carefully, you will see that the spiral terminates before reaching the lateral wall by merging with three topological defects called dislocations. The three convection patterns of Fig. 1.14 raise obvious interesting questions about pattern formation in nonequilibrium systems. Why do we see stripes in one case and hexagons in another? What determines the lattice spacing? Why do the hexagons disappear with a small increase in R, to be replaced by a large rotating spiral? And what determines the angular frequency of the spiral's rotation? We will be able to answer some of these questions in Chapters 6 through 9 later in the book.

The patterns in Fig. 1.14 are time-independent or weakly time-dependent. In contrast, Fig. 1.15 shows snapshots from two different time-dependent states that have been observed in a convecting fluid close to the onset of convection. Figure 1.15(a) shows a most remarkable dynamical state called spiral defect chaos. Spirals and striped regions evolve in an exceedingly complex way, with spirals migrating through the system, rotating (with either sense) as they move, sometimes annihilating with other spirals, and sometimes giving birth to spirals and other defects. It seems almost inconceivable that rising and falling air can spontaneously develop such a complicated dynamical dance, especially under conditions such that the air is constrained by time-independent and spatially homogeneous boundaries. Experiments and numerical simulations have further shown that, under identical experimental conditions (although in a large rectangular convection cell), one can see spiral defect chaos or a time-independent lattice of stripes similar to Fig. 1.14(a), i.e. there are two dynamical attractors and which one is observed depends on the initial conditions of the experiment. So the same fluid can convect in two very different ways under the same external conditions. Another interesting feature of spiral defect chaos is that it is found only in convection systems that are sufficiently big. For geometries with aspect ratio Γ smaller than about 20, one finds other less-disorganized patterns. This dependence on size is not understood theoretically.

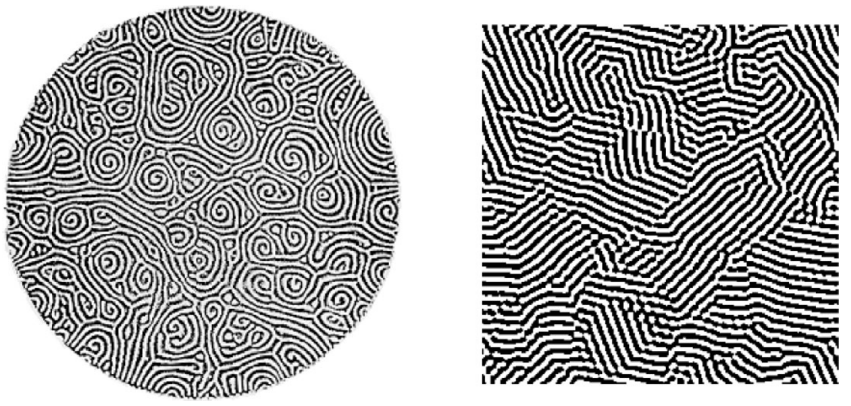

Fig. 1.15 Two spatiotemporal chaotic examples of Rayleigh–Bénard convection. (a) A snapshot of spiral defect chaos in a large cylindrical cell of radius $r = 44$ mm, and depth $d = 0.6$ mm ($\Gamma = 73$), for Rayleigh number $R = 1.894\,R_c$. The fluid is gaseous carbon dioxide at a pressure of 33 bar. (From Morris *et al*. [75]) (b) A snapshot of domain chaos, which occurs in a Rayleigh–Bénard convection cell that is rotating with constant angular frequency about the vertical axis. The figure actually shows results from numerical simulations of equations to be introduced in Chapter 5 but the experimental pictures are similar. Each domain of rolls is unstable to the growth of a new domain with rolls oriented at about 60° with respect to the old angle, and the pattern remains dynamic. (From Cross *et al*. [27].)

If a convection apparatus is rotated at a constant angular frequency ω about its center, a different chaotic dynamics is observed called domain chaos (Fig. 1.15(b)). The rotation rate can be expressed in dimensionless form using a rotational Reynolds number

$$\Omega = \frac{\omega d^2}{\nu}, \tag{1.5}$$

where we use an uppercase Greek omega, Ω, to distinguish this quantity from the Reynolds numbers $\mathcal{R}$ defined in Eq. (1.4) for Couette flow. Provided that Ω exceeds a critical value Ω_c (which has the value $\Omega_c \simeq 12$ for gaseous CO_2), experiments show that the domain chaos persists arbitrarily close to the onset of convection. As the Rayleigh number for convection R approaches R_c from above, the size of the domains and the time for one domain to change into another domain of a different orientation both appear to diverge. The experimental discovery of domain chaos was quite exciting for theorists since, in the regime arbitrarily close to onset, there is a good chance of understanding the dynamics by developing a perturbation theory in the small quantity $\varepsilon = (R - R_c)/R_c \ll 1$.

These two kinds of spatiotemporal chaos raise some of the most difficult conceptual questions concerning sustained nonequilibrium states. How do we understand

such disordered states, as well as the transitions into and out of such states? Are such states analogous to the liquid and gas phases of some equilibrium system and are the transitions between spatiotemporal chaotic states possibly similar to thermodynamic phase transitions? As one example to consider, as the Rayleigh number R is increased with zero rotation rate, a pattern consisting mainly of stripes evolves into the spiral defect chaos state. What then is the effect of rotation on this spiral defect chaos, and how does this state change into domain chaos with increasing Ω?

We now turn away from convection to discuss patterns found in other controlled laboratory experiments. Figure 1.16 shows three new kinds of nonequilibrium

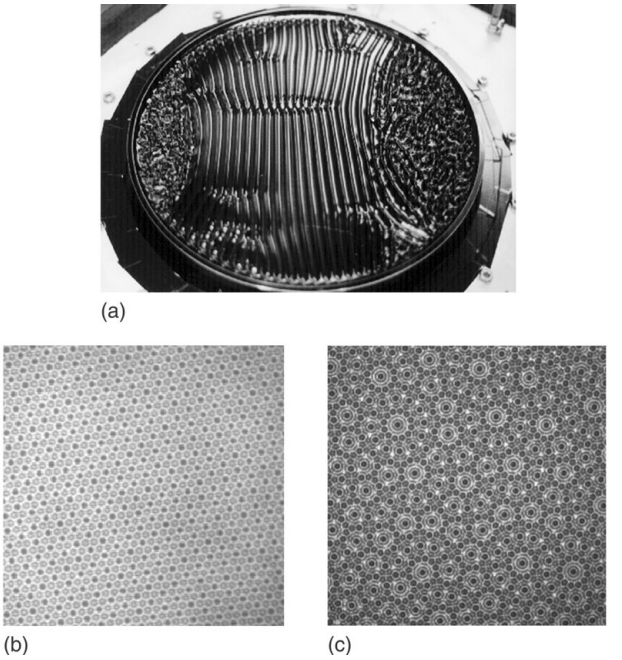

Fig. 1.16 Three patterns observed in crispation experiments, in which a shallow horizontal layer of fluid (here a silicon oil with viscosity $\nu = 1\ \mathrm{cm}^2/\mathrm{s}$) is shaken up and down with a specified acceleration $a(t)$ Eq. (1.6). Bright areas correspond to flat regions of the fluid surface (peaks or troughs) that reflect incoming normal light back toward an imaging device. (a) A mixed pattern of stripe and chaotic regions. The fluid is being driven sinusoidally with parameters $a_1 = 0$ and $a_2 \approx 8g$ (about $1.45a_c$) and $f_1 = 45$ Hz in Eq. (1.6). (From Kudrolli and Gollub [58].) (b) A time-periodic superlattice pattern consisting of two superimposed hexagonal lattices with different lattice constants (ratio $\sqrt{3}$) and rotated with respect to one another by 30°. This figure was obtained by averaging over two drive periods for parameter values $m = 4$, $n = 5$, $a_4 \approx 4.4g$, $a_5 \approx 7.9g$, $f = 22$ Hz, and $\phi = 60°$ in Eq. (1.6). (c) For the same parameters as those of panel (b) but with a relative driving phase ϕ set to 16°, a spatially quasiperiodic pattern is observed that has 12-fold symmetry around various points in the pattern. ((b) and (c) from Kudrolli *et al.* [59].)

patterns that are observed in a so-called crispation or Faraday experiment, named after the British scientist Michael Faraday who was the first to report some observations of such a system in the year 1831. In these particular crispation experiments, a dish containing a fluid layer was shaken up and down with a specified acceleration of the form

$$a(t) = a_n \cos(2\pi nft) + a_m \cos(2\pi mft + \phi). \tag{1.6}$$

Here the acceleration amplitudes a_n and a_m are measured in units of the Earth's acceleration g, the basic frequency f is varied over the range 10–200 Hz, m and n are integers, and ϕ is a specified phase.[6] For the case of sinusoidal driving with $a_n = 0$ and $m = 1$, when the acceleration amplitude a_m or shaking frequency f exceeds some threshold, the fluid's flat surface becomes unstable to the formation of capillary waves (short-wavelength surface waves for which the surface tension of the fluid is a stronger restoring force than gravity) and the nonlinear interaction of these waves leads to intricate patterns, including lattices of stripes, squares, or hexagons, and spatiotemporal chaos.[7] An advantage of crispation experiments over convection and Taylor–Couette experiments is that the effective system size of the system can be easily increased by simply increasing the driving frequency f, which decreases the average wavelength of the patterns.

In Fig. 1.16(a), a cup 32 cm in diameter containing a 3 mm layer of viscous silicon oil was shaken sinusoidally ($a_n = 0$, $m = 1$) with frequency $f = 45$ Hz and acceleration $a_m \approx 8g$. For these parameters, the fluid surface spontaneously evolves to a novel mixed state for which part of the fluid is evolving chaotically and part is an approximately stationary stripe pattern. Unlike the stripe-turbulent state of Fig. 1.11(e), the fronts separating the chaotic and laminar regimes do not propagate. Increasing the amplitude a_1 further causes the chaotic regions to grow in size at the expense of the stripe region until the stripe region disappears completely. These results are not understood theoretically.

The patterns in Figs. 1.16(b) and (c) are obtained for the case of periodic external driving with two frequencies such that the ratio of the driving frequencies is a rational number m/n. If one frequency $f_m = 4f$ is an even multiple and the second frequency $f_n = 5f$ is an odd multiple of a base frequency $f = 22$ Hz, there is a regime of parameters such that the fluid surface spontaneously forms a new kind of structure called a superlattice that can be understood as the superposition of two different lattices. Superlattices are found in other nonequilibrium systems as well

[6] As a simple experiment, you can try placing a loud speaker face up to the ceiling, put a small board on the speaker cone, and then put a cup of water on the board. Playing various tones at different volumes through the speaker will then shake the cup up and down with a prescribed amplitude and frequency and you should be able to see some interesting patterns.

[7] Crispation patterns are all time dependent and vary subharmonically with the driving frequency f. A stationary pattern is then one that looks the same after two driving periods.

as in equilibrium structures. If the relative phase of the driving is decreased from $\phi = 60°$ to 16°, an intricate time-independent pattern is now observed (Fig. 1.16(c)) that is called quasicrystalline since it is spatially nonperiodic yet highly ordered in that its wave number spectrum $P(\mathbf{k})$ has sharp discrete peaks.

Quasicrystalline states are rather extraordinary. Since the development of X-ray crystallography and associated theory in the early twentieth century, scientists had believed that sharp peaks in a power spectrum (corresponding to discrete points in a X-ray film) could arise only from a periodic arrangement of the objects scattering the X-rays. This orthodoxy was proved wrong in 1984 when experimentalists announced the synthesis of the first quasicrystal, an Al-Mn alloy whose X-ray diffraction pattern had the seemingly impossible properties of a 5-fold symmetry (not possible for a space-filling periodic lattice) and sharp peaks (indicating the absence of disorder). Figure 1.16(c) is a nonequilibrium example of a quasicrystalline pattern with a 12-fold symmetry, and experiments show that the pattern is intrinsic since it is not sensitive to the shape or size of the container. Why is panel (c) quasicrystalline rather than striped or hexagonal as we saw for Rayleigh–Bénard convection in Figs. 1.14(a) and (b)? As various parameters are varied, what kinds of transitions into and out of this state exist?

Pattern formation in a rather different kind of crispation experiment is shown in Fig. 1.17, which involves the vertical shaking of a granular medium consisting of thousands of tiny brass balls.[8] This pattern formation is not related to the capillary waves of a Faraday experiment since a granular medium does not possess a surface tension (the brass balls do not attract each other as do the molecules in a fluid). When the dimensionless amplitude of shaking is sufficiently large, the granular layer is actually thrown into the air, somewhat like a pancake from a frying pan, and then the layer starts to spread out vertically since the brass balls are not all moving with identical velocities. It is then possible for the bottom of the container to be moving upwards at the same time as the bottom of the granular layer is descending, causing some balls to strike the bottom (changing their direction) while other balls remain suspended in the air and continue to fall. This can lead to an alternating pattern in which peaks and valleys of balls formed at one cycle become respectively valleys and peaks at the next cycle or every four cycles, and so on.

In Figs. 1.17(a)–(e), we see stripe and hexagonal regions somewhat similar to those observed in convection near onset (Fig. 1.14) but the regions appear in new and unusual combinations, e.g. two kinds of hexagonal regions separated by a front (b), two flat regions (c), a region of locally square cells abutting a stripe region (d), a pattern consisting of three kinds of hexagonal regions (e), and spatiotemporal chaos

[8] This experiment was originally carried out not to study crispation dynamics but to explore the properties of granular media, a major research area of current nonequilibrium science.

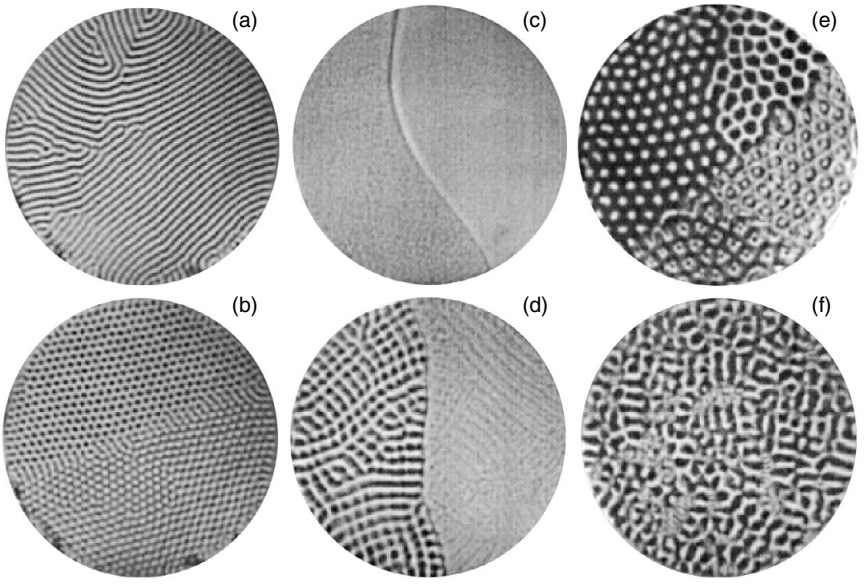

Fig. 1.17 Six patterns observed in a granular crispation experiment. A shallow layer (depth = 1.2 mm) of tiny brass balls (diameters ranging from 0.15–0.18 mm) was vertically shaken up and down in an evacuated cylinder of diameter 127 mm at a constant angular frequency $\omega = 421\ \mathrm{s}^{-1}$ with a varying vertical amplitude A. Each pattern is characterized by the dimensionless acceleration parameter $\Gamma = \omega^2 A/g$ where g is the gravitational acceleration. (a) $\Gamma = 3.3$, a disordered stripe state that is found just above the onset of the instability of a flat uniform state; (b) $\Gamma = 4.0$, a state consisting of two different kinds of locally hexagonal structures; (c) $\Gamma = 5.8$, two flat regions divided by a kink; (d) $\Gamma = 6.0$, a phase of locally square-symmetry states coexisting with a phase of stripes; (e) $\Gamma = 7.4$, different kinds of coexisting hexagonal phases; (f) $\Gamma = 8.5$, a spatiotemporal chaotic state. (From Melo *et al*. [73].)

consisting of short stripe-like domains (f). Unlike convection, Taylor–Couette flow, or crispation experiments with a fluid, it is not clear what sets the length scales of these cellular patterns. The similarities of these patterns to those observed in fluids and in other systems such as lasers is intriguing and puzzling. Is there an underlying continuum description of these brass balls, similar to the Navier–Stokes equations of fluid dynamics? If so, what is that description and how is it derived? What are the properties of the granular media that determine these different spatiotemporal phases?

For our last example of controlled nonequilibrium patterns and dynamics, we discuss experiments involving chemical solutions. Figure 1.18(a) shows a snapshot of a time-dependent two-dimensional chemical reaction known as the Belousov–Zhabotinsky reaction, named after two Russians who, in the 1950s and 1960s,

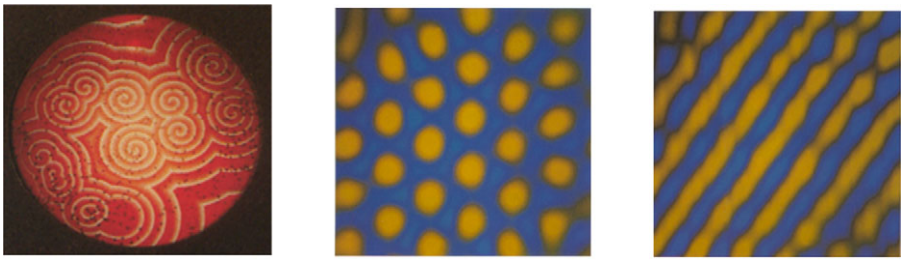

Fig. 1.18 Representative patterns in reaction–diffusion systems. (a) Time-dependent many-spiral state observed in a Belousov–Zhabotinsky excitable reaction consisting of chemical reagents in a shallow layer of fluid in a Petri-like dish. Since the system is closed, the pattern becomes time-independent after a long-lived complicated transient state. (From Winfree and Strogatz [112].) (b) Nearly time-independent hexagonal pattern of spots observed in a chlorite-iodide-malonic-acid (CIMA) system of chemicals that are reacting in a thin cylindrical polyacrylamide gel of diameter 25.4 mm and thickness 2.00 mm. Unlike (a), this is a sustained nonequilibrium system since reagents are fed to and reaction products removed from the gel. The gel suppresses fluid motion and provides a way to visualize the iodide concentration field since the iodide binds with starch embedded in the gel to produce a blue color. The spacing between dots is about 0.2 mm, substantially smaller than the thickness of the gel. (c) For slightly different external conditions, a nearly time-independent stripe pattern is observed instead of comparable wavelength. (From Ouyang and Swinney [84].)

established the remarkable fact that chemical systems could approach equilibrium with a non-monotonic dynamics, e.g. by oscillating in time or by propagating waves in space. When first announced, the experimental discovery was greeted with disbelief and ridicule since most scientists at that time believed incorrectly that the second law of thermodynamics (that the entropy of a system can only increase monotonically toward a maximum value corresponding to thermodynamic equilibrium) implied a monotonic evolution of chemical concentrations toward their asymptotic equilibrium values. With the hindsight of several decades of nonlinear dynamics research that has established convincingly the existence of periodic, quasiperiodic, and chaotic attractors in many experimental systems as well as the occurrence of complicated transients leading to these attractors, it is difficult for contemporary scientists to appreciate this initial disbelief.

Current interest in the Belousov–Zhabotinsky reaction lies primarily in its value as an experimental metaphor for studying more complicated continuous media such as lasers and heart tissue that have the property of being excitable. An excitable medium is such that a local weak perturbation decays while a perturbation whose strength exceeds some threshold grows rapidly in magnitude and then decays. An example is a field of dry grass for which a local increase in temperature causes

no change until the temperature exceeds the kindling point. The temperature then rapidly increases as the grass combusts, a wall of flame propagates through the grass, and then the temperature decays to the ambient temperature once the grass has been consumed. Excitable media such as the Belousov–Zhabotinsky reaction, heart tissue, and dry grass fields show similar spatiotemporal patterns and so investigations of the disordered rotating and propagating spiral waves in Fig. 1.18(a), of target patterns of concentric circular propagating waves (not shown and believed to be induced by impurities such as a piece of dust), and their generalization to three-dimensional chemical media in the form of scroll waves give insight simultaneously to many different systems. The questions of interest are ones that we have discussed earlier in the context of a galaxy's spiral arms and of the aggregation of slime mold. What determines the speed of a front and its frequency of rotation and how do these quantities vary with parameters? For many-spiral states, what happens when one spiral interacts with another spiral or with a boundary? In a three-dimensional medium, what are the possible wave forms and how do their properties vary with parameters?

The reaction–diffusion patterns of Figs. 1.18(b) and (c) involve different chemicals and are qualitatively different in that the medium is not excitable and there are no propagating waves. Also, these figures represent true sustained nonequilibrium states since porous reservoirs in physical contact with opposing circular surfaces of a thin cylindrical gel (see Fig. 3.3 on page 110) feed chemical reagents into the interior of the gel where the pattern formation occurs, and also withdraw reaction products. The small pores of the gel suppress fluid motion which greatly simplifies the theoretical analysis since the spatiotemporal dynamics then arises only from the reaction and diffusion of chemicals within the gel. The patterns were visualized by using the fact that one of the reacting chemicals (iodide) binds to starch that is immobilized in the gel, causing a color change that reflects the local iodide concentration.

A typical experiment involves holding the temperature and reservoir chemical concentrations constant except for one chemical concentration which becomes the control parameter. For one choice of this concentration (Fig. 1.18(b)), the chemicals spontaneously form a locally hexagonal pattern similar to the convection pattern Fig. 1.14(b) and granular crispation patterns in Fig. 1.17. Other parameter values lead to a stripe state, superlattices, and spatiotemporal chaos. These chemical patterns are cellular just like the convection patterns that we discussed in Figs. 1.14 and 1.15 but here the length scale is determined dynamically by a balance of diffusion and chemical reaction rates rather than by the geometry of the container.

When the experiments in Figs. 1.18(b) and (c) and others were first reported around 1990, there was great scientific excitement, not because they were the first examples of nonequilibrium pattern formation but because they were the first to

confirm a remarkable insight of Alan Turing. In 1952, Turing observed that diffusion, which by itself tends to make chemical concentrations spatially uniform, could lead to the formation of cellular patterns if chemical reactions were also to occur. (We will discuss some details of Turing's insight in Chapter 3, when we discuss the linear stability of a uniform state.) Turing then went on to speculate that patterns generated by reaction and diffusion might suffice to explain biological morphogenesis, the formation of structure during the growth of a biological organism. Examples Turing had in mind included the formation of stripes or spots on animal surfaces (tigers, zebras, cheetahs, giraffes, fish, seashells), the formation of symmetrically arranged buds that grow into leaves or tentacles, and the question of how a presumably spherically symmetric fertilized egg (zygote) could start the process of dividing and differentiating into the many different kinds of cells found in an adult organism. Ironically, while Turing's insight of pattern formation by reaction and diffusion was finally confirmed forty years later by nonbiological experiments, pattern formation in biological systems has turned out to be more complicated than originally conceived by Turing, and a picture as simple as the one he proposed has not yet emerged.

1.3.3 What are the interesting questions?

To summarize the many nonequilibrium states discussed in Sections 1.3.1 and 1.3.2, let us list here the scientific questions raised by our discussion:

Basic length and time scales: Many of the patterns that we discussed have a cellular structure, consisting locally of stripes, squares, or hexagons of a certain typical size, or of waves or spirals that evolve with a certain frequency and velocity. An obvious question is what determines the basic length and time scales of such patterns? In some cases such as Taylor–Couette flow and Rayleigh–Bénard convection, the cellular size is determined by the experimental geometry (e.g. the thickness of the fluid layer) but this is not always the case. For example in the limit that the thermal conductivity of a convecting fluid becomes large compared to that of the floor and ceiling in Fig. 1.1 (liquid mercury between two glass plates would be an example), the cellular length scale can become much larger than the depth of the fluid. For reaction–diffusion chemical systems and related media such as the heart or a slime mold, the length and time scales are determined dynamically by diffusion constants and reaction rates.

Wave number selection: For some parameter ranges, stationary spatially periodic lattices are observed that can be characterized by a single number, the lattice spacing. In these cases, we can ask the question of wave number selection: is a unique lattice spacing observed for specified parameters and boundary conditions and what determines its value? If there are multiple spacings, what determines their values?

Related questions arise in other systems. Thus the spirals in spiral galaxies (Fig. 1.4), in slime-mold aggregation (Fig. 1.9), in spiral defect chaos (Fig. 1.15),

and on the surface of a fibrillating heart (Fig. 1.10) all raise the question of what determines the frequency of rotation and the velocity of the arms in the observed spirals. In snowflakes (Fig. 1.8) and in the domain chaos of a convecting fluid (Fig. 1.15), there is propagation of a tip or front and one can ask if the propagation occurs with a unique velocity and what determines that velocity.

You should appreciate that the question of length and time scales and the question of wave number selection are distinct. The question of scales corresponds to knowing what unit of measurement is appropriate (say meters versus millimeters or days versus seconds). The question of wave number selection then corresponds to making precise measurements on this scale. For example, the lattice spacing of hexagonal rolls may be about one millimeter in order of magnitude (the length scale) but in actual experiments we would be interested to know if the precise value is 0.94 or 1.02 mm and whether these values repeat from experiment to experiment.

Pattern selection: For patterns that form in two- and three-dimensional domains, multiple patterns are often observed for the same fixed external conditions. The question of pattern selection is why one or often only a few patterns may be observed or why, in other cases, certain patterns are not observed? An example we discussed above was the occurrence of a spiral defect chaos state (Fig. 1.15(a)) or of a stripe-pattern state under identical conditions in a large square domain. On the other hand, a quasiperiodic pattern like Fig. 1.16(b) has never been observed in a convecting flow. Why not?

Transitions between states: A given nonequilibrium state will often change into some other state as parameters are varied and so we can ask: what are the possible transitions between nonequilibrium states? Of special interest are supercritical transitions – in which a new state grows continuously from a previous state – since analytical progress is often possible near the onset of such a transition.

A related question is whether supercritical nonequilibrium transitions have interesting critical exponents associated with the transition. For second-order thermodynamic phase transitions and for nonequilibrium supercritical transitions, a quantity Q that characterizes the system may converge to zero or diverge to infinity at the transition point as a power law of the form

$$Q \propto |p - p_c|^{\alpha}, \qquad \text{as } p \to p_c, \tag{1.7}$$

where p is the parameter that is being varied with all others held fixed, p_c is the critical value of p at which the supercritical transition occurs, and the quantity α is the critical exponent which determines the rate of convergence or divergence of Q.[9] Some of the great advances in twentieth-century theoretical and experimental science concerned the discovery and explanation for "universal" values of these critical exponents. In equilibrium systems, their values turn out to depend remarkably only on the symmetry

[9] An example of a second-order equilibrium phase transition is the loss of magnetism of pure iron as its temperature T is increased to its Curie temperature $T_c \approx 1043$ K. The magnetization M of the iron decreases to zero according to Eq. (1.7) with an exponent $\alpha \approx 0.3$. The onset of convection in Fig. 1.1 is a supercritical nonequilibrium transition for which the maximum magnitude of the velocity field $\max_{\mathbf{x}} \|\mathbf{v}\|$ vanishes according to Eq. (1.7) with an exponent $\alpha \approx 1/2$.

and dimensionality of the system undergoing the phase transition, but not on the possibly complicated details of its atomic structure. So we can ask: do universal exponents occur in spatially extended nonequilibrium systems? If so, on what details of the system do they depend?

Stability: In addition to classifying the possible transitions between different nonequilibrium states, can we predict when transitions will occur for particular states as particular parameters are varied? For many experiments, the underlying dynamical equations are known and a linear stability analysis of a known state can be attempted numerically (more rarely, analytically). In other cases such as granular flow or neural tissue, the underlying equations are not known (or might not exist or might not be practical to work with mathematically or computationally) and one might instead try to identify empirical features in experimental data that could suggest when a transition is about to occur. Two examples are attempts to predict an economic crash from stock market time series, and efforts to predict the onset of an epileptic seizure from 19-electrode multivariate EEG time series.

Boundaries: Even in experimental systems that are large compared to some basic cellular length scale, the lateral boundaries confining the medium (e.g. the walls in Fig. 1.1) can strongly influence the observed patterns and dynamics. How do the shape, size, and properties associated with lateral boundaries influence the dynamics? One example we discussed in Section 1.3.2 was the fact that spiral defect chaos (Fig. 1.15(a)) is not observed until a convection system is sufficiently wide. Somehow the lateral boundaries suppress this state unless the boundaries are sufficiently far from each other.

Transients: For spatially extended nonequilibrium systems, it can be difficult to determine how long one must wait for a transient to end or even if an observed state is transient or not. Mathematical models of spatially extended systems suggest that the average time for transients to decay toward a fixed point can sometimes grow exponentially rapidly with the system size and so be unobservably long even for systems of moderate size. What determines the time scale for a transient spatiotemporal pattern to decay? Is it possible to distinguish long-lived transient states from statistically stationary states?

Spatiotemporal chaos: Many systems become chaotic when driven sufficiently away from equilibrium, i.e. their nontransient dynamics are bounded, are neither stationary, periodic, nor quasiperiodic in time, and small perturbations grow exponentially rapidly on average. Chaotic pattern forming systems in addition may develop a nonperiodic spatial structure that is called spatiotemporal chaos. Several examples discussed above include spiral defect chaos and domain chaos in Fig. 1.15 and a chaotic pattern in a granular crispation experiment, Fig. 1.17(f). Spatiotemporal chaos raises difficult conceptual questions about how to characterize the spatiotemporal disorder and how its properties depend on parameters.

Transport: For engineers and applied scientists, an important question is how does the transport of energy and matter through a spatiotemporal nonequilibrium system

depend on its parameters? For example, computer chips generate heat and a mechanical engineer may need to design the geometry of a computer board so that convection can remove the heat efficiently. Similarly, the synthesis of an ultrapure crystal from a molten substrate is a nonequilibrium problem for which a chemical engineer needs to know how the transport of impurities into the crystal depends on parameters so that this transport can be minimized.

Control: For many applied science problems, it is not sufficient to observe a nonequilibrium system passively, one needs to control a system actively by applying an external perturbation. An example is the dynamics of left ventricular muscle (Fig. 1.10), for which one might hope to use gentle electrical perturbations to prevent the onset of fibrillation when an arrhythmia appears. Similarly, an electrical engineer may need to apply an external perturbation to a laser to stabilize a regime of high-power coherent emission, or a plasma physicist may want to confine a hot thermonuclear plasma for long times by modulating some external magnetic field, and one can speculate about a futuristic technology that perturbs the atmosphere to prevent the formation of a tornado or hurricane. These goals raise many unsolved questions regarding how a nonequilibrium system responds to external perturbations and how to choose such perturbations to achieve a particular goal.

1.4 New features of pattern-forming systems

The variety of nonequilibrium patterns discussed in the previous sections and the many scientific questions suggested by these patterns are possibly overwhelming if you are learning about these for the first time. To give you some sense about what features of these systems are significant, we discuss in this section some ways that pattern-forming nonequilibrium systems differ from those that you may have encountered in introductory courses on nonlinear dynamics and on thermodynamics. We first discuss some conceptual differences and then some specific new properties.

1.4.1 Conceptual differences

An important new feature of pattern-forming systems and a direct consequence of their nonequilibrium nature is that *the patterns must be understood within a dynamical framework*. This is the case even if we are interested in just time-independent patterns such as panels (a) and (b) of Fig. 1.14. In strong contrast, the geometry and spacing of a spatial structure in thermodynamic equilibrium can be understood as the minimum of the system's energy (or, more precisely, as the minimum of the system's free energy for systems at a finite temperature T). A familiar equilibrium example is a periodic lattice of atoms or molecules in a crystal. The positions of the atoms can be determined directly from the energy of their mutual

interaction, independently of the dynamics of the atoms, since the minimum energy is achieved for zero velocity of each atom and so depends only on the positions of the atoms.[10] This is not the case for nonequilibrium systems *since generally there is no free-energy-like quantity whose extremum corresponds to the static nonequilibrium pattern*. (We will discuss this point in more detail later in the book but note for now that the absence of a free energy is partly a consequence of the fact that nonequilibrium systems are open systems subjected to imposed external fluxes and so a system's energy, mass, and momentum are often not conserved.) Furthermore, we are often interested in the breakdown of stationary patterns to new patterns that remain dynamic indefinitely, a phenomenon that obviously requires a dynamical formulation and that has no thermodynamic analogy.

Introductory nonlinear dynamics courses discuss systems that are well described with just a few variables, e.g. the logistic map, the Hénon map, the standard map, the driven Duffing equation, and the Lorenz model. A pattern-forming system differs fundamentally in that many variables are needed to describe the dynamics (the phase space is high-dimensional). New concepts and methods are then needed to study pattern formation, and indeed many basic ideas that you may have learned in an introductory nonlinear dynamics course will not be applicable in this book. For example, the strategy of studying a continuous-time dynamical system via its associated discrete-time Poincaré map is no longer useful, nor is it productive to analyze an experimental time series by embedding it into some low-dimensional phase space. As mentioned above, a high-dimensional phase space is needed even to describe a fixed point (an attractor with zero fractal dimension) such as the static pattern of convection rolls in Fig. 1.14(a) since the transient orbit meanders through the high-dimensional space as it approaches the fixed point.

Figure 1.19 gives a physical insight into why pattern-forming systems have a high-dimensional phase space by contrasting two convection systems. The thermosyphon shown in Fig. 1.19(a) is a thin closed circular pipe filled with a fluid that is heated over its bottom half and cooled over its top half. From our discussion of convection in Section 1.2, you will not be surprised to learn that if the circular pipe is placed vertically in a gravitational field, then for a temperature difference between the top and bottom halves that exceeds some critical value, the fluid begins to circulate around the tube, forming a simple convection "roll." (Which way does the fluid begin to circulate? This is not determined *a priori*, and the circulation will be clockwise for some experimental runs, anticlockwise for others – a good example of what is known as a broken symmetry.) If the temperature difference in

[10] We are thinking about the atoms classically here, a good approximation except for the lightest atoms such as hydrogen and helium. In a full quantum mechanical description the atoms are no longer at rest in the crystal even at zero temperature due to zero point motion. However, the lattice structure is still obtained as the minimum energy state, albeit involving a more complicated calculation of the energy.

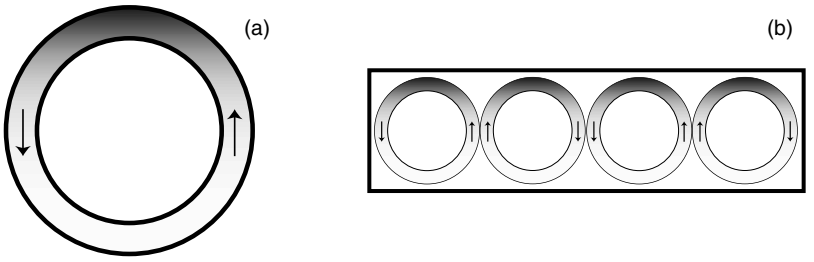

Fig. 1.19 Two convection systems: (a) a thermosyphon and (b) Rayleigh–Bénard convection with many rolls. The light and dark regions denote respectively warm and cool fluid regions. The thermosyphon is well-described by attractors in a three-dimensional phase space whereas the patterns in Rayleigh–Bénard convection require a high-dimensional dynamical description even to describe its static states.

this simple system is set to some still larger value, the direction of flow shows spontaneous chaotic reversals at what appear to be random time intervals. And indeed experimentalists have shown that these reversal events are described well by the three-variable Lorenz equations, one of the most famous systems in the study of low-dimensional chaos.[11] We can easily understand why a three-variable description might be adequate for Fig. 1.19(a). Although there are other dynamical degrees of freedom of the fluid such as variations of the flow transverse to the axis of the pipe, these turn out to be rapidly damped to constant values by the fluid viscosity since the walls are close together and the fluid velocity is zero at the wall. Thus these transverse degrees of freedom do not enter into the thermosyphon dynamics.

This thermosyphon should be contrasted with the pattern-forming convection system in Fig. 1.19(b). Roughly, we might consider each convection roll to be analogous to a separate thermosyphon loop so that the dimension of the phase space needed to describe the convection system will be proportional to the number of convection rolls (or alternatively proportional to the length of the convection experiment). In fact, if we drive this system at a strength corresponding to the onset of chaos in the thermosyphon, we would find that we not only have to include for each roll three Lorenz-type variables of circulation velocity, temperature perturbation and heat flow, but also new variables associated with distortions of each roll caused by the coupling of each roll to other rolls. A pattern like Fig. 1.14(a) with about 40 rolls may then well involve a phase space of dimension at least 150, huge compared to any dynamical system described in introductory nonlinear dynamics courses. We will indeed have to develop new concepts and methods to work with such high-dimensional phase spaces.

[11] The Lorenz variables X, Y, and Z are now interpreted as the fluid circulation velocity, the asymmetry of temperature between the right and left halves of the loop, and the heat transported.

By the way, Fig. 1.19 illuminates another (although somewhat technical) point, that the essential difference between the two convection systems is not that the thermosyphon is described by a few coupled ordinary differential equations while the convection system is described by a few coupled partial differential equations (abbreviated throughout this book as pdes). This might appear to be the case since dynamical systems described by partial differential equations in principle have infinite-dimensional phase spaces with the dynamical variables specified at a continuum of points labeled by their position in space. In fact, both systems in Fig. 1.19 are described by the partial differential equations of fluid dynamics and heat transport. However for the thermosyphon, the dynamics of interest can be understood within a truncated approximation of a few important dynamical degrees of freedom (because of the strong damping by nearby lateral walls), whereas the interesting dynamics in the pattern-forming system, such as the approach to a stationary state or the transition of a stationary state to persistent dynamics, cannot. In Chapter 6, we will see that even reduced descriptions of pattern-forming systems are often described by partial differential equations (amplitude equations) and so remain infinite dimensional.

We have argued that an important difference between the dynamical systems studied in an introductory nonlinear dynamics course and the pattern-forming systems discussed in this book is that a description of the latter requires a high-dimensional phase space. This is all well and good but you may ask, is there some easy way to determine the phase-space dimension of an experiment or of a simulation? Fortunately, there are two informal ways to estimate whether some system has a high-dimensional phase space. One is simply visual inspection. If a nonequilibrium system is large compared to some basic characteristic length (e.g. the width of a convection roll), then a high-dimensional phase space is likely needed to describe the dynamics. We will call such systems spatially extended. A second way to identify a high-dimensional phase space is to simulate the system on a computer. If many numerical degrees of freedom are needed (e.g. many spatial grid points or many modes in a Fourier expansion) to reproduce known attractors and their bifurcations to some reasonable accuracy, then again the phase space is high-dimensional.

Using visual inspection to estimate whether the phase space of some system is high-dimensional assumes that we somehow know some characteristic length scale with which we can compare the size of an experimental system. Identifying such a length can be subtle but is often clear from the context of the system being studied. As we have seen in Section 1.3, many pattern-forming systems involve cellular structures (e.g. stripes and hexagons) or propagating waves in the form of spirals or scroll waves which all have a well-defined wavelength. In these cases, a system is spatially extended with a high-dimensional phase space if its geometric size is large compared to the size of this wavelength. For more strongly driven nonequilibrium

systems, there can be structure over a range of length scales[12] and often no single length can be identified as being special (for example, in Fig. 1.11(d), there is structure on length scales substantially smaller than the width of a Taylor cell). But then the fact that there is structure over a range of lengths itself indicates the need for a high-dimensional phase space. For strongly driven systems we might need to introduce other length scales called correlation lengths that quantify over what distance one part of the system remains correlated with another part. A system is spatially extended and high dimensional if it is geometrically large compared to any one of these correlation lengths.

The high-dimensional phase space of pattern-forming systems has the unfortunate implication that data analysis is challenging, both technically and conceptually. Current desktop spatiotemporal experiments and simulations may require storing and analyzing hundreds of gigabytes of data as compared to a few tens of megabytes for low-dimensional dynamical systems. Several satellite-based observational projects investigating the dynamics of Earth's ecology, geology, and meteorology are approaching hundreds of terabytes in storage. By comparison, the total printed contents of the Library of Congress constitute about 10 terabytes and several independent estimates suggest that the amount of information stored in the human brain over a lifetime is perhaps 1–10 gigabytes of compressed data. There is then a great need for theoretical insight that can suggest ways to reduce such vast quantities of data to manageable amounts and to identify questions that can be answered. We will touch on some of these data analysis issues several times throughout the book but you should be aware that these are difficult and unsolved questions.

Closely related to the challenge of analyzing large amounts of spatiotemporal data is the challenge of simulating spatially extended dynamical systems. In an introductory nonlinear dynamics course, no sophistication is needed to iterate a map with a few variables or to integrate the three-variable Lorenz equations for a long period of time, one simply invokes a few appropriate lines in a computer mathematics program like Maple or Mathematica. But to integrate numerically in a large box the partial differential equations that describe Rayleigh–Bénard convection (the Boussinesq equations) for the long times indicated by experiments is much more challenging. One can rarely look up and just use an appropriate algorithm because there are numerous subtleties concerning how to discretize three-dimensional time-dependent nonlinear partial differential equations and how to solve the related linear algebra problems efficiently (which may require solving hundreds of millions of

[12] A "range of length scales" can be made more quantitative and objective by Fourier analyzing some observable $u(\mathbf{x}, t)$ associated with the system and then by calculating the time-averaged wave-number spectrum $P(k)$. The range of length scales then corresponds to the range of wave numbers $[k_1, k_2]$ such that $P(k)$ differs significantly from zero.

simultaneous linear equations at each successive time step). Writing, validating, and optimizing an appropriate code can take several years, even for someone with a Ph.D. with special training in computational science. Further, even if a validated code were instantly available, powerful parallel computers are needed to simulate such equations in large domains over long time scales and such computers are still not widely available or easy to use.

1.4.2 New properties

In addition to a high-dimensional phase space, spatially extended sustained nonequilibrium systems have some genuinely new features when compared to dynamical systems that evolve only in time. One such feature concerns how a fixed point becomes unstable. For a system that evolves only in time (e.g. a driven nonlinear pendulum), an infinitesimal perturbation of an unstable fixed point simply grows exponentially in magnitude (or perhaps exponentially with oscillations if the imaginary part of the growth rate is nonzero). But for pattern-forming systems, an infinitesimal perturbation of an unstable fixed point can grow spatially as well as temporally. Further, there are two distinct kinds of spatial growth. One kind is an absolute instability in which a perturbation that is localized over some region of space grows at a fixed position. The second kind is a convective instability in which the instability propagates as it grows. For this second kind of instability, there is exponential growth only in a moving frame of reference. At any observation point fixed in space, there is growth and then asymptotic decay of the instability as the propagating disturbance moves beyond the observation point.

The linear instability of the uniform motionless state of air to convection rolls in the convection experiment Fig. 1.1 is an example of an absolute instability. The instability of snowflake dendritic tips in Fig. 1.8 is an example of a propagating convective instability. This convective instability explains why no two snowflakes are ever alike since it has the remarkable property of magnifying noise arising from the molecular collisions near the tip of the growing dendrite. Perturbations from this noise later influence the formation of the dendrite's side branches.

Another new property is that a large pattern-forming system can consist of different spatial regions that each, by itself, could be a pattern for the entire system. Further, such a quilt of different states can persist for long times, possibly indefinitely. An example is Fig. 1.16(a), where a region of nearly time-independent stripes coexists with chaotic disordered regions. Similarly, Fig. 1.17 shows several quilt-like patterns, e.g. a square lattice adjoining a hexagonal lattice, each one of which could fill the entire domain on its own. The localized region of a system separating one pattern from another is called a front. Theoretical progress can often be made by analyzing fronts as separate and simpler dynamical systems.

1.5 A strategy for studying pattern-forming nonequilibrium systems

As you now appreciate from the above examples and discussion, the scope of nonequilibrium physics is actually enormous since any system that is not in thermodynamic equilibrium is by definition a nonequilibrium system. Necessarily, the phenomena we discuss in a book must be limited and in this section we describe the kinds of nonequilibrium systems that we do and do not consider and also a strategy for investigating the systems of interest.

We will be concerned primarily with nonequilibrium systems that are maintained in a state away from thermodynamic equilibrium by the steady injection and transport of energy. Most interesting to us are systems displaying regular or nearly regular spatial structures, some examples of which we discussed in Section 1.3. We will discuss stationary spatial structures, their breakdown to persistent dynamical states that are also disordered in space, and also systems supporting propagating spatial structures. A major focus of this book is also on systems that may be investigated by precise, well-controlled laboratory experiment and for which there is a well-understood theoretical formulation. The idea is to learn about the complex phenomena of nonequilibrium systems through the study of these systems ("prepared patterns"), exploiting the close connection between theory and experiment. The ultimate goal is then to apply this knowledge to a wider range of problems ("natural patterns"), perhaps where experimental intervention such as changing parameters is not possible (e.g. the climate and many biological systems).

Figure 1.20 provides a way to understand how the systems described in this book fit into the broader scheme of sustained nonequilibrium systems. A particular nonequilibrium system can be thought of as occupying a point in a three-dimensional parameter space with axes labeled by three dimensionless parameters R, Γ, and N that we discuss in turn.

The parameter R is some dimensionless parameter like the Rayleigh number, Eq. (1.1), that measures the strength of driving compared to dissipation. For many systems, driving a system further from equilibrium by increasing R to larger values leads to chaos and then to ever-more complicated spatiotemporal states for which there is ever finer spatial structure and ever faster temporal dynamics. A canonical example of a large-R system is highly turbulent fluid flow, e.g. the flow generated behind a propeller rotating at high speeds. When discussing Fig. 1.6, we saw that the Sun's turbulent outer layer corresponds to a Rayleigh number of order 10^{12} so there are some systems for which the R-axis can span at least 12 orders of magnitude.

Some nonequilibrium systems disintegrate or change their properties when driven too strongly and so cannot be driven to arbitrarily large values along the R axis. Examples might be a laser that burns through confining mirrors if pumped too strongly, a biological system that becomes poisoned and dies if given too much

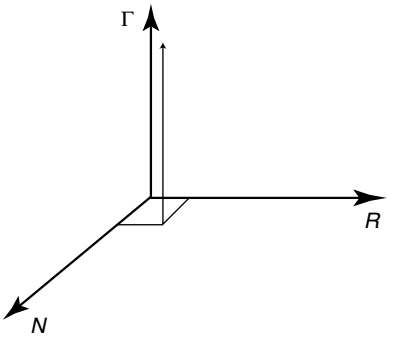

Fig. 1.20 A parameter space for categorizing sustained spatially extended nonequilibrium systems. The R-axis is the "driving" or fluid-dynamics axis that measures how far a system has been driven from equilibrium. The Γ axis is the "size" or pattern-forming axis, indicating the size of a system relative to some basic length scale such as the depth of a fluid. The N axis is the number of distinct components that interact and can be thought of as the "biological" axis since living systems have large numbers of different interacting components. Most of what is currently known about nonequilibrium systems involves regions for which at least two of the three variables R, Γ, and N are small. Most of this book will concern the regime of small N, small R, and large Γ as indicated by the thin vertical arrow.

of some nutrient like salt, or the medium in a crispation experiment that might be thrown clear from its container if shaken up and down too strongly. Also some systems have stress parameters that simply cannot be raised above some finite value. An example would be the concentration of some reagent that drives a solution of reacting chemicals out of equilibrium. The concentration cannot be increased indefinitely since, at some point, the solution becomes saturated and the reagent starts to precipitate. Since fluids are the most widely studied systems that can be driven strongly out of equilibrium, we can think of the R-axis in Fig. 1.20 as also being a "fluid dynamics" axis.

The vertical axis labeled by Γ (upper-case Greek gamma) is the "aspect ratio" axis, and indicates how large a system is compared to some characteristic length scale such as the size of some cellular structure or the depth of the medium. We can also consider this axis to be the "pattern-forming" axis since for larger Γ (bigger systems), the influence of lateral confining boundaries is reduced and the phenomenon of pattern formation becomes more clear. Nonequilibrium desktop experiments using liquid crystals as a medium have attained values of Γ as large as 1000 while numerical simulations in one-space dimension have reached $\Gamma \approx 10\,000$. These might seem like impressively large values but you should keep in mind that crystals can be considered to have a much bigger aspect ratio of order $1\,\text{cm}/10^{-7}\,\text{cm} \approx 10^7$ (ratio of macroscopic crystal size to its lattice spacing), so nonequilibrium experiments are not yet "macroscopic" compared to their characteristic length scale.

Earth's ocean and troposphere (layer of the atmosphere closest to Earth where the weather evolves) both have a depth of about 10 km and a lateral expanse of order the radius of the Earth (6400 km) and so are big nonequilibrium systems with $\Gamma \approx 600$.

The Γ-axis is important because experiments have shown that simply increasing the system size with all other parameters held fixed can induce interesting dynamics such as a transition from a stationary to chaotic behavior. This was first shown in a seminal experiment of Guenter Ahlers and Robert Behringer in 1978, when they studied the dynamics of a convecting fluid (liquid helium at the cryogenic temperature of 4 K) just above the onset of convection for several cylindrical containers whose aspect ratios Γ (ratio of radius to depth) varied from $\Gamma = 2.1$ to $\Gamma = 57$. Ahlers and Behringer then discovered that simply making a convection system larger and larger for a fixed Rayleigh number was sufficient to cause the dynamics to eventually become chaotic. This discovery has since been verified more carefully and in other nonequilibrium systems and is now considered a general, although poorly understood, feature of sustained nonequilibrium systems. We note that although many systems cannot be driven strongly from equilibrium, at least in principle all nonequilibrium systems can be made arbitrarily large. Exploring the large-Γ limit is therefore experimentally and theoretically interesting for many nonequilibrium systems.

Finally, the third axis labeled N indicates the number of distinct components that interact at each point in a given system. This number can usually be determined by inspection of the mathematical equations (if known) by simply counting the number of distinct fields. For example, a complete mathematical description of a Rayleigh–Bénard experiment involves five coupled fields – the fluid pressure $p(\mathbf{x}, t)$, the fluid temperature $T(\mathbf{x}, t)$, and the three components of the fluid's velocity field $v_i(\mathbf{x}, t)$ for $i = x$, y, and z – and so $N = 5$ for a convecting fluid. Biological, ecological, economic, and chemical systems are often characterized by large values of N so one can think of the N-axis as the "biological" axis for the space of nonequilibrium systems. Nonequilibrium systems with large values of N are perhaps the least well understood and are associated with some of the most interesting current scientific questions. Did life arise on Earth by a spontaneous self-organization in some primordial soup consisting of many chemicals? What determines the number of species in a large ecosystem? How do the many genes coordinate their dynamics and so guide the development of an organism over its lifetime? How does a human brain of 10^{10} neurons assemble itself and how do these neurons with their network of 10^{13} connections act dynamically to produce our cognitive abilities of pattern recognition, associative memory, language, and creative thinking?

Figure 1.20 suggests a simple strategy for investigating nonequilibrium systems, which is to allow only one of the three variables N, R, and Γ to become large at a time. (In contrast, the physical systems studied in an introductory nonlinear

dynamics course correspond to having all three variables small or moderate at the same time, and many of the natural systems discussed in Section 1.3.1 have all three variables large at the same time.) This book is largely concerned with phenomena for large values of Γ, and small to moderate values of N and R, as indicated by the thin vertical arrow near the Γ-axis in Fig. 1.20. Although this regime might seem excessively restricted, experiments like those discussed in Section 1.3.2 show that there is an enormous richness of dynamics in this regime and so there is, if anything, an excess of phenomena to understand. Much future work will be needed, however, to explore the regimes corresponding to two or three of these variables having large values simultaneously.

In this book, we will therefore study mainly systems with large Γ and moderate values of R and N. However, there are some further assumptions to make if we are to obtain experimental systems that are as simple as possible and for which the associated theory is manageable. We will emphasize experimental systems that:

(i) **are large** in one or more spatial directions so that the influence of lateral boundary conditions on pattern formation can be reduced, simplifying subsequent theoretical analysis.

(ii) **are homogeneous** so that the pattern formation is intrinsic rather than driven by inhomogeneities. Coating the floor and ceiling of a room with flat uniform layers of copper (Fig. 1.1) was an example of how an experimental system could be made spatially homogeneous. Studying convection over a bumpy floor would be less instructive than convection over a homogeneous floor since the bumps influence the pattern formation and their influence would have to be studied as a separate problem.

(iii) **involve few fields** (small N) which reduces the mathematical and computational effort. For nearly all examples discussed in this book, N will be 6 or less.

(iv) **have local space-time interactions**, a technical mathematical assumption that the dynamical equations involve only fields and finitely many spatial and temporal derivatives of the fields. This assumption is mainly a convenience for theorists and computational scientists since it reduces the mathematical effort needed to analyze the system. Most systems discussed in Section 1.3 have such local interactions so this assumption is not a severe restriction. An example of a nonequilibrium system with nonlocal interactions would be neural tissue since a given neuron can connect to remote neurons as well as to neighboring neurons. Further, there are various time delays associated with the finite propagation speed of signals between neurons. The dynamics then depends nonlocally on information over some time into the past and the mathematical description involves delay-differential equations that can be hard to analyze.

All the systems we will discuss in detail satisfy these basic criteria. In addition the following conditions are also desirable. The systems should

(i) **be described by known equations** so that quantitative comparisons between theory, numerics, and experiment are feasible;
(ii) **be well characterized**, for example the parameters changing the behavior should be easily determined, and the geometry and boundary conditions should be accurately prescribed; and
(iii) **permit easy diagnosis**, allowing accurate quantitative measurements of one or more of the fields relevant to the pattern formation.

Historically, fluid systems have been found to approach many of these ideals. First, many fluid systems have few interacting components (velocity and pressure and sometimes temperature or concentration fields). Second, the fluid dynamics is described by mathematical equations such as the Navier–Stokes equations that experiments have confirmed to be quantitatively accurate over a large range of parameters. Third, the fluid equations involve just a few parameters such as the kinematic viscosity ν or thermal diffusivity κ and these parameters can be measured to high accuracy by separate experiments in which issues of pattern formation do not arise. Fourth, fluids are often transparent and so visualization of their spatial structure is possible at any given time. Finally, experiments have shown that many phenomena observed in non-fluid nonequilibrium experiments often have some analog in a fluid experiment so one can study general features of nonequilibrium phenomena using some fluid experiment.

Of all the possible fluid experiments, Rayleigh–Bénard convection has been especially favored in basic research because the fluid is in contact with time-independent and spatially homogeneous boundaries that are especially easy to characterize and to maintain. In other fluid experiments (e.g. Fig. 1.11 or Fig. 1.16), the fluid is set in motion by some pump or motor that oscillates and these oscillations can be an additional source of driving that complicates the identification of intrinsic pattern formation. We do note that steady technological improvements allow increasingly well-controlled experiments on more exotic systems such as chemical reactions in a gel layer (fed by opposing reservoirs) or on a carefully prepared rectangular slab of heart muscle. The possibilities for careful comparisons between theory and experiment are rapidly improving.

1.6 Nonequilibrium systems not discussed in this book

For lack of space, time, and expertise, we cannot reasonably address all the nonequilibrium systems that have been studied or even all the systems that have received the deep scrutiny of the research community. Some of the topics that we will leave out include the following:

Quenched states: If the driving of a nonequilibrium system is turned off sufficiently quickly or if a parameter describing some equilibrium system is abruptly changed

to some new value (e.g. if the temperature of a liquid is quickly decreased below its freezing point), the system can "freeze" into a so-called quenched state that is often disordered and that can take a long time to return to thermodynamic equilibrium. Quenched states are technically nonequilibrium but differ from the systems discussed in this book in that they are not sustained systems. There are many interesting questions concerning how a quenched state approaches its usually ordered equilibrium limit, e.g. by the formation of small ordered domains that grow in size at certain rates. Two examples of quenched states are glass (like that found in a window) and a soap-bubble foam that coarsens over time.

Pattern formation by breakdown: Some patterns in nature are formed by some stress slowly increasing to the point that some threshold is crossed, at which point the medium relaxes quickly by creating a pattern. Examples include cracks propagating through a brittle material, electrical breakdown of an insulator from a high-voltage spark, and the occurrence of an earthquake in response to the buildup of stress in a tectonic plate.

Fully developed fluid turbulence: In our discussion of Fig. 1.20 above, we observed that fluids are one of the few continuous media that can be driven strongly out of equilibrium. There is in fact extensive theory, experiment, and applications in the fully developed fluid turbulence regime of large R, moderate N, and moderate Γ. However a reasonable discussion would be lengthy and technical to the point of almost requiring a book of its own. Also, the subject of high-Reynolds-number turbulence is sufficiently special to fluids that it falls outside our intent to discuss mainly ideas and mechanisms that apply to several nonequilibrium systems.

Adaptive systems: Economic, ecological, and social systems differ from many of the systems discussed in the book in that the rules under which the components interact change over time, the systems can "adapt" to changes in their environment. One example is the evolutionary development of language and increased intelligence in *homo sapiens* which greatly changed the rules of how humans interact with each other and with the world.

1.7 Conclusion

This has been a long but important chapter. We have introduced and discussed representative examples of pattern formation and dynamics in sustained nonequilibrium systems, and have identified questions to pursue in later chapters. The experimental results discussed in Section 1.3 are an especially valuable source of insight and direction since mathematical theory and computer simulations still lag behind experiment in being able to discover the properties of pattern-forming systems. In the following chapters, we develop the conceptual, analytical, and numerical frameworks to understand sustained nonequilibrium spatially extended systems.

1.8 Further reading

(i) A comprehensive and broad survey of pattern-formation research, although at a more advanced level than this book, is "Pattern formation outside of equilibrium" by Cross and Hohenberg [25]. This article is a good place to find discussions of pattern-forming systems that are not mentioned in this book, to see deeper discussions of pattern-forming systems, and to see many applications and discussions of theory to experimental systems.
(ii) Many examples of patterns are discussed at a non-technical level in the book by Ball *The Self-Made Tapestry: Pattern Formation in Nature* [9].
(iii) An introductory article on the large-scale structure of the Universe is "Mapping the universe" by Landy [61].
(iv) Many beautiful photographs showing the enormous diversity of snowflakes can be found in the book *The Art of the Snowflake: A Photographic Album* by Libbrecht [64].
(v) A classic paper in pattern formation in chemical reactions and the possible relevance to morphogenesis is Turing's "The chemical basis of morphogenesis" [106].
(vi) A history of pattern formation in chemical systems is given in the first chapter of Epstein and Pojman's book [34]. If you have access to a chemistry laboratory, you can explore the Belousov–Zhabotinsky reaction by following the recipe given in the appendix of the book by Ball [9].
(vii) For an introduction to low-dimensional dynamical systems see *Nonlinear Dynamics and Chaos* by Strogatz [99].

Some articles on specific topics discussed in this chapter (in addition to those referenced in the figure captions) are listed below.

(i) The thermosyphon: "Nonlinear dynamics of a convection loop: a quantitative comparison of experiment with theory" by Gorman *et al*. [41].
(ii) Cracks and fracture patterns: "How things break" by Marder and Fineberg [68].
(iii) The importance of aspect ratio in the onset of chaos: "The Rayleigh–Bénard instability and the evolution of turbulence" by Ahlers and Behringer [1].
(iv) Spiral defect chaos: "Spiral defect chaos in large-aspect-ratio Rayleigh–Bénard convection" by Morris *et al*. [77].

Exercises

1.1 **End of the Universe:** In Section 1.1, the interesting structure of the Universe was traced to the fact that the Universe was still young and evolving. But will the Universe ever stop expanding and reach an equilibrium state? If so, what kind of structure will exist in such a Universe? What might happen to the Universe in the long term has been discussed in a fascinating article "Time without end: Physics and Biology in an open universe" by the physicist

Freeman Dyson in the article *Reviews of Modern Physics* **51**, 447 (1979). Read this article and then answer the following questions:

(a) What is the difference between an "open" and "closed" universe and what are the implications for whether the universe will ever reach thermodynamic equilibrium?
(b) What experimental quantities need to be measured to determine whether our Universe is open or closed? According to current experimental evidence, is our Universe open?
(c) According to Dyson, how long will it take our Universe to reach thermodynamic equilibrium, assuming that it is open?
(d) Can life, as we know it on Earth, persist arbitrarily into the future if our Universe is open and approaching an equilibrium state?

1.2 **Just six numbers:** In the book *Just Six Numbers: The Deep Forces That Shape the Universe* (Basic Books, New York, 1999), cosmologist Martin Rees argues that our Universe can form interesting patterns – and life in particular – only because certain key parameters that describe the Universe fall within extremely narrow ranges of values. For example, one parameter is the fractional energy $\varepsilon = 0.004$ released when four hydrogen nuclei fuse to form a helium nucleus in the core of a star. If this value were just a tiny bit smaller, condensing clouds of gas would never ignite to become a star. If just a tiny bit bigger, stars would burn up so quickly that life would not have enough time to evolve.

Skim through this book and explain briefly what are the six parameters that Rees has identified as being critical to the existence of pattern formation in the Universe. Discuss qualitatively how the Universe would be different from its present form if these parameters had significantly different values.

1.3 **A sprinkling of points: pattern or not?** Like the stars in Earth's sky, some patterns are less a geometric lattice (or distortions of such a lattice) than a statistical deviation from randomness. To explore this point, assume that you are given a data file that contains the coordinates (x_i, y_i) of 4000 points in a unit square (see Fig. 1.21). Discuss how to determine whether these dots constitute a "pattern" or are "random," in which case we would not expect any meaningful structure. What are some hypotheses that a random distribution would satisfy? How would you test the consistency of the data with your hypotheses? Two possibilities to explore are a chi-squared test [89] and a wave-number spectrum.

1.4 **Properties of the Rayleigh number:** Answer the following questions by thinking about the criterion Eq. (1.1) for the onset of convection.

(a) Two identical convection systems of depth d are filled with air and mercury respectively at room temperature. Using the values in Table 1.1, determine

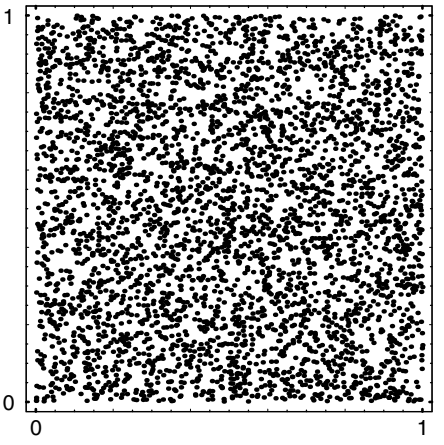

Fig. 1.21 Exercise 1.3: Do these 4000 dots in a unit square constitute a "pattern" that deviates statistically from points thrown down randomly and uniformly?

which fluid will start to convect first as the temperature difference ΔT is increased in small constant steps through onset.

(b) The bottom plate of a certain wide square convection cell is machined to have a square bump that is 5% of the fluid depth in height and four times the depth of the fluid in width as shown schematically in this figure:

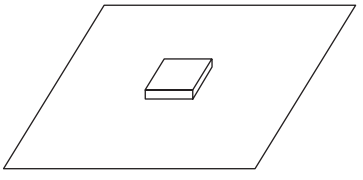

The bump is far away from the lateral walls. As the temperature difference is increased in small constant steps starting with the stable motionless fluid, where will convection first start in this system? Guess and then sketch what kind of pattern will be observed when the convection rolls first appear.

1.5 **Suitability of a room for a convection experiment:**

(a) Assume that the room in Fig. 1.1 has a height of $d = 3$ m, that the floor and ceiling are isothermal surfaces of temperature T_1 and T_2 respectively (both close to room temperature $T = 300$ K), and that high-precision laboratory experiments can control a temperature difference to at best about one part in 10^4. Determine whether or not this room is suitable for convection experiments.

(b) An unstated assumption for almost any laboratory experiment is that the experiment can be finished within a practical amount of time, say a week or

less. Theory discussed later in the book shows that one of the slowest time scales associated with convection is the so-called vertical thermal diffusion time $t_v = d^2/\kappa$, where d is the depth of the fluid and κ is the fluid's thermal diffusivity. This is the time for a localized temperature perturbation near, say, the bottom plate to be detected by a probe near the top plate if the perturbation spreads out purely by diffusion. There is an even longer time scale called the horizontal thermal diffusion time $t_h = (L/d)^2 t_v = \Gamma^2 t_v$, which is the time taken for a localized temperature perturbation on one side of the system to be detected on the far side of the system a lateral distance L away if the perturbation again spreads out purely by diffusion. Any given convection experiment, or simulation of such an experiment, needs to span many multiples of these time scales in order for enough time to pass that transients die out and a statistically stationary state is attained.

1. What are the times t_v and t_h in units of days for air in a square room of height $d = 3\,\text{m}$ and width $L = 8\,\text{m}$? Are these reasonable time scales for a convection experiment?
2. Answer these same questions for air in a laboratory convection apparatus with $d = 1\,\text{mm}$ and $L = 5\,\text{cm}$.

1.6 **Temperature profile and heat transport of a conducting fluid:**

(a) For Rayleigh numbers in the range $0 < R < R_c$, plot the vertical temperature profile $T(z)$ of the air in Fig. 1.1. Assume $z = 0$ is the floor and $z = d$ is the ceiling.

(b) For this same regime of Rayleigh number, plot the heat flux $H = H(R)$ (heat energy per unit area per unit time) through the ceiling.

(c) To get a feeling for the order of magnitude of the heat transport, estimate the total heat transported by the air through the ceiling for a square room of height $d = 3\,\text{m}$ and width $L = 5\,\text{m}$, when the temperature difference is the critical value ΔT_c. For comparison, a typical room heating device has a power consumption of a few kilowatts (thousands of joules per second).

(d) When $R > R_c$ so that the air in Fig. 1.1 starts to convect, discuss and sketch qualitatively how the temperature profile and total heat transport will change.

(e) Invent and explain a method to measure the instantaneous heat flux $H(t)$ experimentally for a fixed Rayleigh number R.

Hint: For a continuous medium with thermal conductivity K the heat flux is $H = -K\,\nabla T$ (units of energy per unit time per unit area). Assuming most of the air in the room is close to room temperature $T = 293\,\text{K}$, you can use the value $K = 2.5 \times 10^{-6}\,\text{J}\,\text{m}^{-1}\,\text{s}^{-1}\,\text{K}^{-1}$ everywhere inside the room.

1.7 **Scaling of time, length, and magnitude scales for the Swift–Hohenberg equation:** To gain experience simplifying a dynamical equation and identifying dimensionless parameters, consider the following partial differential equation for a real-valued field $u(x,t)$ that depends on time t and one spatial coordinate x:

$$\tau_0\,\partial_t u(x,t) = ru - \xi_0^4\Big(q_0^4 + 2q_0^2\,\partial_x^2 + \partial_x^4\Big)u - g_0u^3. \tag{E1.1}$$

This is the so-called Swift–Hohenberg equation which we will discuss in Chapters 2 and 5 as one of the more important models of pattern formation. Eq. (E1.1) seems to have five distinct parameters, namely the time scale τ_0, the coherence length ξ_0, the critical wave number q_0, the nonlinear strength g_0, and the control parameter r.

By a clever choice of time, length, and magnitude scales t_0, x_0, and u_0, i.e. by changing variables from t, x, and u to the scaled variables τ, y, and v by the equations

$$t = t_0\tau, \quad x = x_0 y, \quad u = u_0 v, \tag{E1.2}$$

and by redefining the parameter r to a new value $\hat{r}$, show that Eq. (E1.1) can be written in a dimensionless form with only *one* parameter:

$$\partial_\tau v = \hat{r}v - \left(1 + 2\,\partial_y^2 + \partial_y^4\right)v - v^3. \tag{E1.3}$$

This is a substantial simplification since the mathematical and numerical properties of this equation can be explored as a function of a *single* parameter $\hat{r}$.

1.8 **Applications of the Reynolds number:** For problems in which an isothermal fluid flows through a pipe or past an object like a cylinder, an analysis of the Navier–Stokes equations reveals a dimensionless stress parameter called the Reynolds number $\mathcal{R}$,

$$\mathcal{R} = \frac{vL}{\nu}, \tag{E1.4}$$

where v is a characteristic magnitude of the fluid's velocity field (say the maximum speed of the fluid before it encounters some obstacle), L is the size of the object with which the fluid interacts (e.g. the diameter of the pipe or of the cylinder), and ν is the kinematic viscosity of the fluid, the same parameter that appears in the Rayleigh number Eq. (1.1).

For small flow speeds corresponding to $\mathcal{R} < 1$, the fluid is usually laminar, i.e. time independent and without an interesting spatial structure (the stream lines are approximately parallel). For Reynolds numbers larger than about 1, laminar flows usually become unstable and some new kind of pattern or dynamics occur. When $\mathcal{R}$ becomes larger than about 1000, the fluid often becomes chaotic in time and irregular in space.

The following questions give you a chance to appreciate the many useful predictions that can be made by studying a parameter like Eq. (E1.4).

(a) Show that the Reynolds number is a dimensionless quantity and so has the same value in any system of units.
(b) For an airplane traveling at $v = 500\,\text{km/hour}$, will the air flow over the wing be laminar or turbulent?
(c) As you walk around a room, show that the air in the vicinity of your foot will be turbulent. This implies that a cockroach will need some way to locate your foot in the midst of a turbulent flow to avoid being stepped on.
(d) By flipping a coin, estimate the speed with which it falls and the speed with which it rotates and then determine whether fluid turbulence plays a role in the supposedly "random" behavior of flipping a coin to call heads or tails.
(e) From a human physiology book or from the web, find the typical speed of blood flowing through your arteries and through your heart. Does the blood flow in any of your arteries become turbulent? What about through a heart valve?
(f) When the wind blows transversely past a telephone wire, you sometimes hear an eerie whistling sound called an aeolian tune. Using the kinematic viscosity of air at room temperature from Table 1.1 and a wire diameter of $L = 2\,\text{mm}$, what is the smallest wind velocity for which you would expect to hear an aeolian tune?

1.9 **Simple experiment to demonstrate the no-slip fluid boundary condition:** To convince yourself of the fact that a fluid's velocity goes to zero at a material wall in the frame of reference of that wall, try the following simple experiment. Get a desktop fan and sprinkle some talcum powder (or any fine powder) over the blades of the fan. Then turn the fan on so that the blades rotate at high speed for several seconds and switch off the fan. Has the talcum powder been blown completely off the blades?